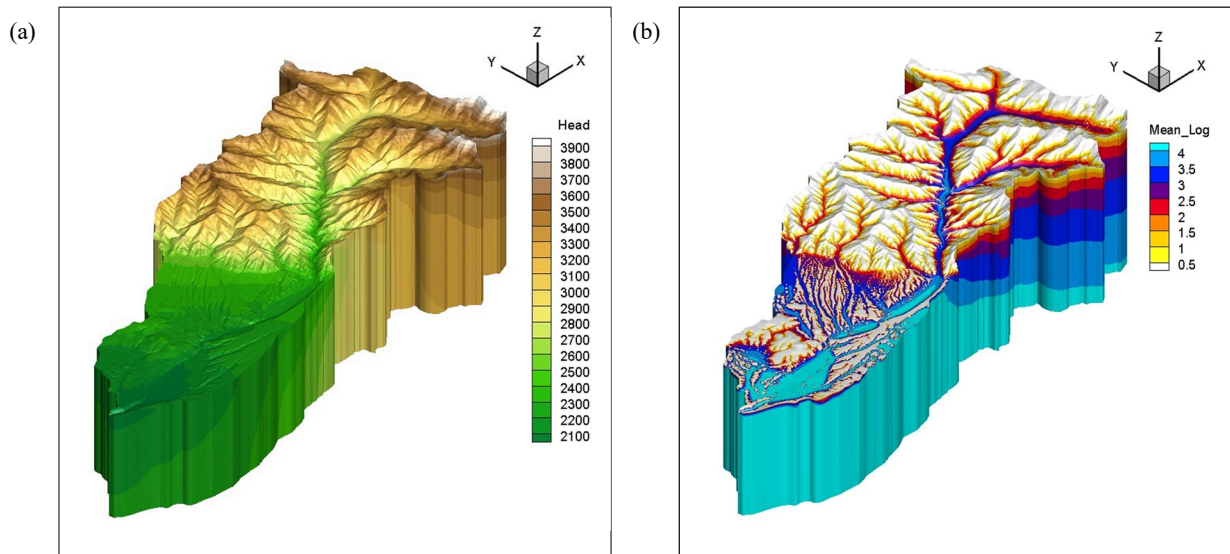February 2019

NEW MEXICO'S MOUNTAIN SOURCES OF WATER: A MECHANISTIC APPROACH TO UNDERSTAND MOUNTAIN RECHARGE AND ITS IMPLICATIONS FOR LOCAL AND STATEWIDE WATER BUDGETS

Jesus Gomez-Velez
Chao Wang

Simulated steady-state groundwater (a) head and (b) mean age (unit: day) in the Rio Hondo watershed under fully saturated conditions (page 19)

New Mexico's Mountain Sources of Water: A Mechanistic Approach to Understand Mountain Recharge and Its Implications for Local and Statewide Water Budgets

By

Jesus Gomez-Velez, Assistant Professor
and
Chao Wang, PhD Candidate

Technical Completion Report
Account Number 126931

February 2019

New Mexico Water Resources Research Institute
in cooperation with the
Hydrology Program, Department of Earth & Environmental Science
New Mexico Tech

Contents

DISCLAIMER

The purpose of the New Mexico Water Resources Research Institute (NM WRRI) technical reports is to provide a timely outlet for research results obtained on projects supported in whole or in part by the institute. Through these reports the NM WRRI promotes the free exchange of information and ideas and hopes to stimulate thoughtful discussions and actions that may lead to resolution of water problems. The NM WRRI, through peer review of draft reports, attempts to substantiate the accuracy of information contained within its reports, but the views expressed are those of the authors and do not necessarily reflect those of the NM WRRI or its reviewers. Contents of this publication do not necessarily reflect the views and policies of the Department of the Interior, nor does the mention of trade names or commercial products constitute their endorsement by the United States government.

ACKNOWLEDGEMENTS

ABSTRACT

We investigate the controlling mechanism of stream network structure, topography, geology and climate in hydrological processes and recharge in mountainous watersheds. The first part of the work explores in detail the importance of capturing key topographic features for modeling groundwater flow and transport in mountainous watersheds. We simulate baseflow, mean age, and the concentration of solute from subsurface chemical weathering for different levels of representation of streams and ridges in the mesh. The topography complexity level (TCL), a measure of our ability to resolve topographic features, is increased progressively by refining the mesh along more streams and ridges of lower Horton-Strahler orders. Our results show that TCL controls the proportion of baseflow generated from local, intermediate and regional flow paths. Ignoring lower-order streams or ridges diminishes flow through local flow paths and biases higher the contribution of intermediate and regional flow paths. Consequently, it results in baseflow mean age being biased older. The magnitude of the bias increases for systems where permeability rapidly decreases with depth giving the dominance of shallow flow paths. Based on a simple geochemical model, the concentration of weathering product is less sensitive to the TCL due to the thermodynamic constraints on chemical reactions. Interestingly, slowly depth-decaying permeability enhances, while rapidly depth-decaying permeability diminishes, the effect of TCL on solute concentration, due to the change of the relative magnitude of mean age and chemical equilibrium time. The second part of the work uses synthetic watersheds to explore the controlling mechanism of the landscape structure on groundwater flow and transport, baseflow generation, and recharge estimation. Preliminary results show that channel network and topographic structure can significantly influence the spatial distribution of baseflow across stream order, and the recession rate of baseflow. Our results will improve baseflow recession analysis, which is a critical step in building parsimonious recharge estimation models based-on watershed storage-discharge relationships.

Keywords: Groundwater recharge, topography, stream network structure, geology, climate, mountainous watersheds

Chapter 1

INTRODUCTION AND JUSTIFICATION OF WORK PERFORMED

Recharge is an important component of the water budget, and therefore its quantification at local and regional scales is critical for water resources management under current and future conditions. In semiarid environments, such as New Mexico, mountain recharge represents a significant fraction of the total recharge to basin aquifers. With this in mind, a detailed mechanistic understanding of the "mountain's internal plumbing" is critical to adequately quantify recharge fluxes.

The aim of this project is to implement fully-coupled groundwater-surface water, three-dimensional models for four watersheds along a climatic and geologic gradient in New Mexico. Given the complexity of the project and the emergence of new and valuable scientific questions during the project, we focused on the Rio Hondo watershed first (this report), and future work will implement similar analysis for the remaining watersheds. These watersheds are located in areas where a significant effort is currently underway to estimate recharge rates within the context of a project focusing on a statewide recharge map for New Mexico. These models will be used to quantify mountain recharge and explore the limits of applicability of a parsimonious approach that can be easily applied at regional scales, and therefore support the efforts to estimate a recharge map for the State.

For the studied watershed, the high-complexity model is used as a learning tool to quantify the relative importance of (i) topography and river network structure, (ii) geology, (iii) soil cover and vegetation, and (iv) weather and climate. This report presents detailed results on quantifying the importance of topography and river network structure and geology in simulating the internal flow and transport processes in mountainous

watersheds. We develop model scenarios of different topographic complexity levels (TCLs) by progressively capturing more streams and ridges with mesh refinement. Homogeneous and exponentially-decaying hydraulic conductivity fields are used to represent different geological heterogeneities (i.e., bedrock permeability conditions). The effect of capturing topographic features on groundwater circulation and the spatial patterns of baseflow and its mean age and solute concentrations are analyzed. Our results reveal the importance and mechanism of topography and river network structure in controlling the internal flow and transport processes, which is a crucial step toward building parsimonious recharge estimation model based on watershed storage-discharge relationship and water balance principle. We also present some initial results of estimating soil cover depth based on topography, which will be included in future analysis when the vadose zone processes will be considered in recharge estimation.

The high-complexity models is being used to project how future climatic change might impact mountain recharge in the state of New Mexico. Some initial results on baseflow generation under the control of different topographic structure under prolonged drought scenario are presented. Precipitation events with different intensity, duration, and interval will be implemented in future analysis to represent different future climate scenarios, and the spatial distribution of recharge under different topography and geology conditions will be mapped.

Chapter 2

REVIEW OF METHODS USED

2.1 Study Site: Rio Hondo Watershed

The Rio Hondo watershed is located in Taos, northern New Mexico. This watershed is part of the Sangre de Cristo mountain system and has a relief of over 2 km, with a maximum elevation of 4,013 m.a.s.l at Wheeler Peak and a lower elevation of 1,971 m.a.s.l at the outlet of the watershed in the Taos valley (Figure 2.1).

The mountain block and the mountain valley have distinct geological conditions (Tolley, 2014; Frisbee et al., 2017). The mountain block is steep and rugged, with slopes ranging from 0 to 72° and a geology dominated by highly fractured (without preferential fracture orientation) crystalline basement rock composed of Precambrian gneisses, schists, and mafic metavolcanics with Tertiary granodiorite to granite intrusions (Figure 2.2), and a lithology of quartz monzonite, felsic gneiss, amphibolite, quartzite, and minor quartz mica schist. The highly fractured bedrock and steep topography favors a topographically driven groundwater flow system with groundwater circulation depth down to probably as great as 2.5 km (Frisbee et al., 2017). In contrast, the mountain valley is relatively flat and dominated by alluvial sediments of the Santa Fe group and young basalt flows (Figure 2.2).

The Rio Hondo watershed is located in a temperate semiarid climate region. Distinct temperature and precipitation conditions can be found in the mountain block and mountain front valley regions due to the topographic difference. The average daily temperature in the mountain block and mountain valley floor ranges from -25 to 17 °C and -1 to 31 °C, respectively. The mean annual precipitation in the mountain block ranges from 48.2 to 99.0 cm, while the mean annual precipitation in the mountain valley floor ranges from 28.0 to 45.7 cm. About 45-55% of the annual precipitation in the watershed occurs in the winter and
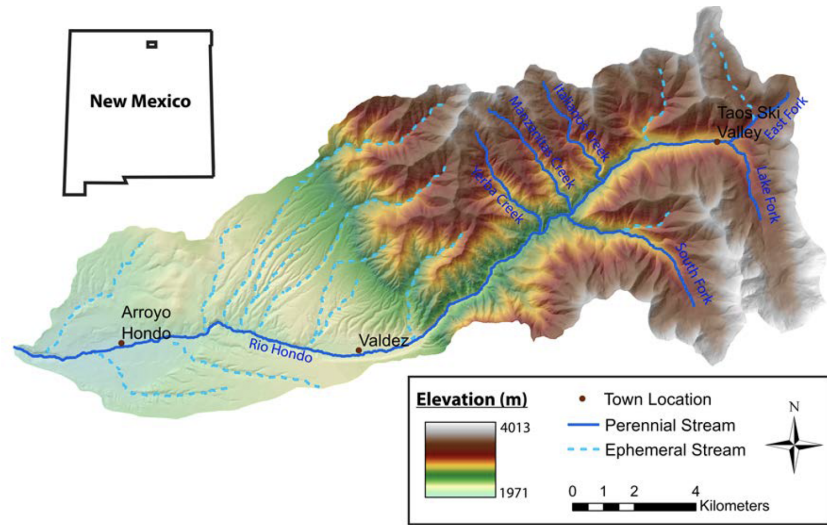
Figure 2.1: Topography of the Rio Hondo watershed with major perennial and ephemeral streams (from Tolley, 2014).
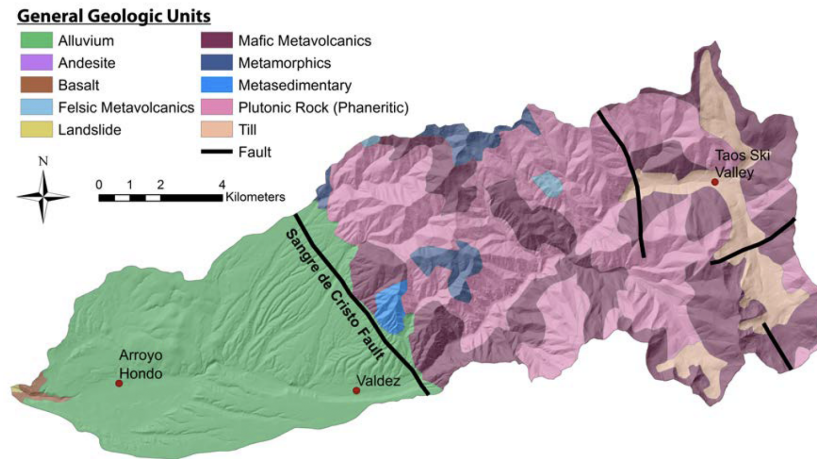
Figure 2.2: Spatial distribution of general geologic units and major faults in the Rio Hondo watershed (Compiled by Tolley, 2014).

spring, with the remainder occurring in the summer monsoon season from July to September. About 33% of the precipitation falls as snow in the mountains, and 13-18% falls as snow in the mountain valley floor. End member mixing analysis shows that most of the recharge is sourced from the snowmelt, while very little recharge occurs in the monsoon season despite the large component of annual precipitation during that season (Tolley, 2014).

## 2.2 Effect of Capturing Topographic Features on Groundwater Modeling

2.2.1 Model Configuration and Subsurface Heterogeneity

To explore the effect of capturing topographic features on groundwater modelling, we use the topography of the Rio Hondo, which is a typical mountainous watershed with steep and complex topography characterized by significant contributions of deep groundwater to streamflow that tend to increase with drainage area (Tolley, 2014; Tolley et al., 2015; Frisbee et al., 2017). The hydrological and geochemical trends observed in this watershed are consistent with the conceptualization of a three-dimensional, topography-driven groundwater flow system (Tóth, 1963; Tóth, 2009) and a three-dimensional catchment mixing watershed conceptual model (Frisbee et al., 2011). Thus the Rio Hondo watershed provides an ideal testbed to explore the effect of capturing topographic features on groundwater modelling with the aid of numerical experiments that are generic in nature and allow us to generalize our conclusions.

Our analyses use the topography of the Rio Hondo watershed (i.e., topographic template) with different geological heterogeneity scenarios (i.e., geologic template), effectively generating a series of distinct systems where we explore the effect of mesh resolution in detail. Our systems include one homogeneous and six heterogeneous hydraulic conductivity fields, resulting in a total number of seven. To this end, we use an exponentially decaying isotropic hydraulic conductivity conceptualization (Louis, 1972) (Fig. 2.3a):

$$K(\mathbf{x}) = K_0 \exp[-\gamma d(\mathbf{x})] \tag{2.1}$$

where K_0 is the hydraulic conductivity at the surface [LT^{-1}], $d(\mathbf{x})$ is depth below land surface [L] with $\mathbf{x} = [x, y, z]$ the coordinate vector [L], and γ is a decay rate [L^{-1}]. The decay rate can be used to define the extinction depth $d_e = 1/\gamma$ [L], which represents the depth where the hydraulic conductivity is approximately 37% of the surface value (i.e., an e-fold decrease). For all simulations $K_0 = 7.438 \times 10^{-5}$ m $\cdot$ s^{-1}, representative of sand, and $\gamma \in \{0.001, 0.003, 0.01, 0.03, 0.1, 0.3\}$ m^{-1} ($d_e \in \{1000, 333.3, 100, 33.3, 10, 3.3\}$ m), consistent with previous studies (Ingebritsen and Manning, 1999; Saar and Manga, 2004; Cardenas and Jiang, 2010). Equation (2.1) allows us to mimic systems that range from shallow, hillslope-dominated flow in the critical zone to deep flow in permeable fractured bedrock (Fig. 2.3b).
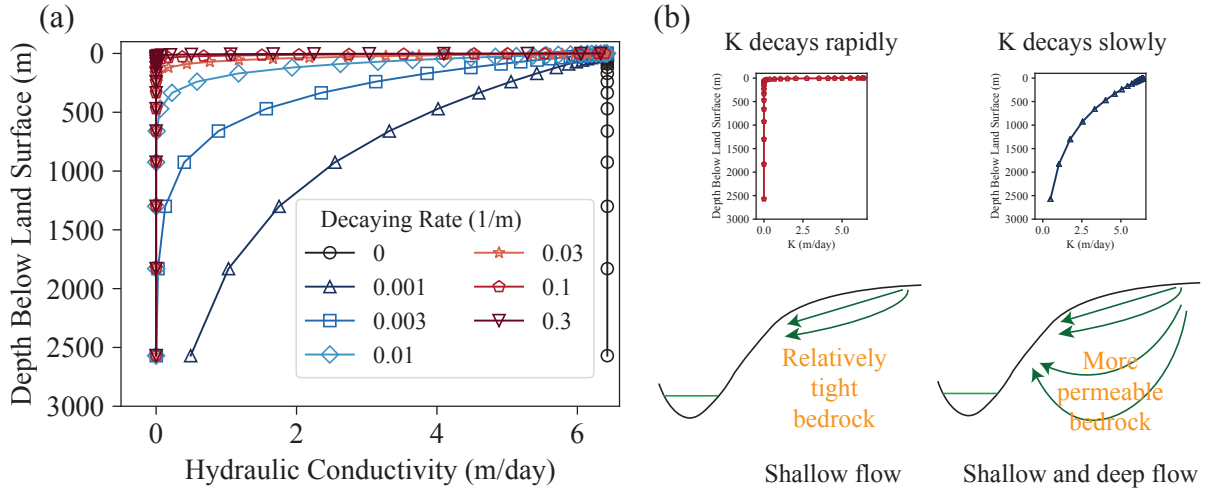
Figure 2.3: (a) One homogeneous and six exponentially-decaying hydraulic conductivity scenarios representing different geological conditions. (b) Flow path distributions within two representative hillslope cross-sections. For hillslopes with hydraulic conductivity decaying relatively slowly with depth, both shallow and deep groundwater flow are present in the system. For hillslope with hydraulic conductivity decaying rapidly with depth, shallow flow dominates the system.

Topographic Complexity Scenarios

We generate a series of meshes that capture topographic variations with different degrees of fidelity by maintaining a constant value for the largest element size and progressively increasing resolution along selected streams and ridges – we refer to this process as increasing *Topographic Complexity Level*, TCL. To this end, a Digital Elevation Model (DEM) for the Rio Hondo watershed, with a resolution of 1/3 arc-second, is obtained from the USGS National Elevation Dataset (NED, https://nationalmap.gov/elevation.html. The DEM is hydrologically corrected (Tarboton et al., 1991) and streams and ridges of subwatersheds up to order 5 are extracted using the Hydrology toolset implemented in Esri® ArcGIS®. The extracted stream network is then used as a template to generate meshes with varying TCLs.

First, we discretize the watershed into a two-dimensional (2-D) triangular mesh using Leapfrog® Geo. The maximum node spacing (80 m), constant for all the topographic complexity scenarios, is determined as half the average divide-to-stream distance of the watershed, which is approximated as half the reciprocal of drainage density (Horton, 1932; Rodríguez-Iturbe and Rinaldo, 1997; Dingman, 2015). Second, to capture local scale topographic variability, we prescribe mesh nodes with a finer resolution (20 m) along the polylines that define the streams and ridges. Using this approach, we increase the topographic complexity level, or TCL, by progressively including lower-order channels and their corresponding ridges. For example, TCL1S, the lowest complexity level, only refines the mesh along the fourth- and fifth-order streams and TLC1SR refines the same streams as TLC1S plus their corresponding ridges. Finally, TLC4SR, the highest

6

Table 2.1: Deficit of detailed topographic information (i.e., stream and ridge features ignored) for models of different topographic complexities relative to the model with the highest complexity, TCL4SR

TCL	Streams Ignored	Ridges Ignored
1S	3, 2, 1	5, 4, 3, 2, 1
1SR	3, 2, 1	3, 2, 1
2S	2, 1	5, 4, 3, 2, 1
2SR	2, 1	2, 1
3S	1	5, 4, 3, 2, 1
3SR	1	1
4S	-	5, 4, 3, 2, 1
4SR	-	-

complexity level, refines the mesh along all the streams and ridges from order 1 to 5. Refinement features for the TCLs explored are shown in Fig. 2.4, and features not captured by each TCL are summarized in Table 2.1.
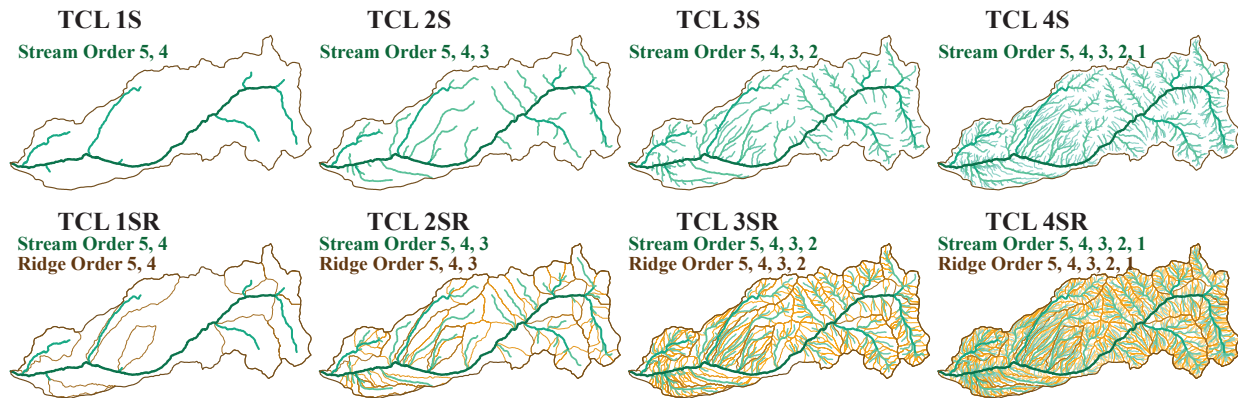
Figure 2.4: Streams (green lines) and ridges (brown polygons) used for mesh refinement. Each topographic complexity level (TCL) refines the mesh along corresponding linear features. TCL4S captures all the streams and is used as an "ideal" base case to evaluate models with other meshes missing some streams. TCLiclSR ($icl = 1, 2, 3, 4$) are used to evaluate the effect of missing ridges.

Finally, each triangular mesh is extruded vertically to create 3-D triangular prism elements. The bottom of the modeling domain is 3000 m below land surface. The simulation domain is vertically divided into 29 parallel layers, with layer thickness increasing exponentially downward, ranging from 0.1 m for the top layer to 860 m for the bottom layer.

Groundwater Flow

For each geological heterogeneity scenario, groundwater flow is simulated with each of the TCL meshes. Given that our focus is on topography-driven groundwater flow and its implications for baseflow generation and solute transport, we simulate saturated steady-state groundwater flow and assume that the water table is

a subdued replica of the land surface elevation (i.e., the terrain elevation corresponds to the prescribed head at the top boundary) (Tóth, 1963; Freeze and Witherspoon, 1967; Haitjema and Mitchell-Bruker, 2005). Lateral and bottom boundaries are assumed to be impervious. The mathematical statement under these assumptions is given by

$$\nabla \cdot [K \nabla h] = 0 \tag{2.2}$$

$$h(x, y, z = z_0(x, y)) = z_0(x, y) \quad \text{on} \quad \partial \Omega_1 \tag{2.3}$$

$$\vec{n} \cdot [K \nabla h] = 0 \quad \text{on} \quad \partial \Omega_2 \text{ and } \partial \Omega_3 \tag{2.4}$$

where h is hydraulic head [L], K is hydraulic conductivity [LT^{-1}], z_0 is land surface elevation [L], $\vec{n}$ is the outward normal vector at the boundary, $\partial \Omega_1$ is the top boundary, $\partial \Omega_2$ is the lateral boundary, and $\partial \Omega_3$ is the bottom boundary.

The mathematical statement (2.2)-(2.4) is solved with HydroGeoSphere (HGS) (Therrien et al., 2010), a physically based, fully integrated surface-subsurface 3-D flow and transport code based on a control volume finite element method.

Groundwater Age

Similarly, for each geological heterogeneity scenario, mean age is simulated with each of the TCL meshes. The mathematical statement for the mean age A [T] is given by

$$-\nabla \cdot \vec{q} A + \nabla \cdot \theta \vec{D} \nabla A + \theta = 0 \quad \text{in} \quad \Omega \tag{2.5}$$

$$A = 0 \quad \text{on} \quad \partial \Omega_1 \tag{2.6}$$

$$\vec{n} \cdot (\vec{q} A - \theta \vec{D} \nabla A) = 0 \quad \text{on} \quad \partial \Omega_2 \text{ and } \partial \Omega_3 \tag{2.7}$$

where $\vec{q} = -K \nabla h$ is the Darcy flux vector [LT^{-1}], $\vec{D}$ is macro-dispersion tensor [L^2 T^{-1}], and θ is porosity [-]. We used HGS to solve (2.5)-(2.7), and a detailed description of the theory and application of age distributions and their moments can be found in Goode (1996); Varni and Carrera (1998); Ginn (1999); Gomez and Wilson (2013).

2.2.2 Metrics

Baseflow into Streams

We use baseflow to evaluate the effect of TLC on flow patterns under various geological scenarios. Simulated water flux leaving the domain through the top boundary $\partial\Omega_1$ (i.e., groundwater discharge) is assigned to a stream node, using the topography, and treated as baseflow. Total baseflow into a stream i of order ω for a given TCL mesh ($cl \in \{1S, 1SR, ..., 4S, 4SR\}$) is calculated as:

$$Q_{b,\omega,i}^{cl} = \sum_{j \in \Omega_{node}^{\omega,i}} |Q_j| \tag{2.8}$$

where $\Omega_{node}^{\omega,i}$ is the set of nodes draining into stream $l_{\omega,i}$, determined with the flow directions estimated during the subwatershed extraction, and with $Q_j < 0$, which indicates flux out of the domain. $i = 1, 2, ..., N_\omega$ with N_ω the number of streams of order ω and $\omega = 1, 2, ..., 5$ for the Rio Hondo watershed. Total flux discharging into streams for the entire stream network is calculated as:

$$Q_{b,T}^{cl} = \sum_{\forall Q_j < 0} |Q_j| \tag{2.9}$$

We use expressions (2.8) and (2.9) to propose a normalized baseflow for each stream $l_{\omega,i}$:

$$\rho_{b,\omega,i}^{cl} = \frac{Q_{b,\omega,i}^{cl}}{Q_{b,T}^{cl}} \tag{2.10}$$

Finally, to evaluate the effect of capturing more lower-order streams, we calculate the relative difference of the normalized baseflow between models of TCL $iclS$ (icl=1,2,3) and the model with mesh capturing all streams (TCL4S):

$$\Delta\rho_{b,\omega,i}^{iclS} = \left(\frac{\rho_{b,\omega,i}^{iclS} - \rho_{b,\omega,i}^{4S}}{\rho_{b,\omega,i}^{4S}}\right) \times 100\% \tag{2.11}$$

Similarly, the effect of capturing ridges is evaluated by comparing results of meshes TCLiclS and meshes TCLiclSR (icl=1,2,3,4)

$$\Delta\rho_{b,\omega,i}^{iclSR} = \left(\frac{\rho_{b,\omega,i}^{iclS} - \rho_{b,\omega,i}^{iclSR}}{\rho_{b,\omega,i}^{iclSR}}\right) \times 100\% \tag{2.12}$$

Flushing Intensity

The flushing intensity (Zlotnik et al., 2011; Gomez-Velez et al., 2014), an integrated measure of the capacity of the flow system to transport water mass by advection at different depths, is used:

$$F(z) = \frac{1}{S}\iint_S \sqrt{(q_x^2(\vec{x}) + q_y^2(\vec{x}) + q_z^2(\vec{x}))}\,ds \tag{2.13}$$

where S is the area of the layer over which the magnitude of flux is integrated. The flushing intensity of models with different TCLs are compared with the base case model under the same geologic condition.

Baseflow Mean Age

Similar to the baseflow, we estimate the flux-weighted mean age of baseflow for each stream $l_{\omega,i}$ as:

$$A_{b,\omega,i}^{cl} = \frac{1}{Q_{b,\omega,i}^{cl}} \sum_{j \in \Omega_{node}^{\omega,i}} |Q_j| A_j. \tag{2.14}$$

Relative difference of mean age for each stream $\Delta A_{b,\omega,i}^{iclS}$ [%] and $\Delta A_{b,\omega,i}^{iclSR}$ [%] is calculated in the same manner as Equations (2.11) and (2.12) between models of different TCL and the reference models.

Chemical Weathering Flux

The relative magnitude of groundwater residence time compared to the time required for mineral weathering to reach equilibrium controls the concentration of solutes from chemical weathering in catchments, influences chemical evolution of stream water, and influences CO_2 emission and thus earth's temperature (Maher, 2011; Maher and Chamberlain, 2014). Using the analytical solution of a 1-D advection-reaction equation to describe the solute concentration along one particular flow path, and assuming an exponential distribution of groundwater residence times, Maher and Chamberlain (2014) proposed a lumped model describing the mean solute concentration C [M L^{-3}] at the catchment outlet:

$$C = C_{eq}\frac{\tau Da}{1 + \tau Da} = C_{eq}(1 - \frac{1}{1 + \tau Da}) \qquad (2.15)$$

where C_{eq} [M L^{-3}] is the thermodynamic limit of equilibrium concentration, $\tau = \exp(2) \approx 7.4$ is a scaling factor, which ensures the concentration from one particular flow path to reach 99.9% of C_{eq} when the travel time equals the equilibrium time in the analytical solution of the 1-D advection-reaction equation, and Da is the Damköhler number, which is the ratio of the mean fluid travel time to the time required to reach chemical equilibrium:

$$Da = T_f/T_{eq} \qquad (2.16)$$

where T_f [T] is mean fluid travel time, and T_{eq} [T] is the equilibrium time for chemical weathering, which is the ratio of equilibrium concentration C_{eq} to the reaction rate R_n [ML^{-3}T^{-1}]. The reaction rate R_n can be estimated to be the maximum reaction rate $R_{n,max}$ [ML^{-3}T^{-1}] times the fraction of fresh minerals f_w, which is assumed to be 1 in this study. We use a value of $C_{eq} = 380\ \mu$ mol/L and $R_{n,max} = 1085\ \mu$ mol/L/yr, representative of SiO$_2$ (see SI in Maher and Chamberlain, 2014, for detailed values of these parameters).

We assume that the residence time distribution for fluid parcels at each nodal point in our model can be approximated as exponential but with mean value $T_f = A_{b,\omega,i}^{cl}$ and use this lumped model to calculate the solute concentration at each nodal point to test the sensitivity of solute concentration to change of mean residence time caused by different mesh TCLs. A discharge weighted average of solute concentrations of water draining from all nodal points into one stream is calculated to be the mean solute concentration of that stream. Results for models with different TCLs are compared in the same manner as Equations (2.11) and (2.12) to evaluate the effects of mesh TCL on stream chemistry.

2.2.3 HydroGeoSphere

We use the model HydroGeoSphere (HGS) to solve the groundwater flow and mean age equations. HGS is an integrated surface-subsurface hydrological model that fully couples 2-D surface flow and transport equations with the 3-D variably saturated subsurface flow and transport equations (Therrien et al., 2010; Brunner and Simmons, 2012). HGS simulates surface flow using the 2-D vertically integrated diffusion-wave approximation of the Saint Venant equation. The variably saturated subsurface flow is governed by the 3-D Richard's equation. The classical advection-dispersion equation is used for solute and thermal transport

11

in both surface and subsurface domains. A more detailed description of the theory and application of HGS can be found in Aquanty (2016).

The surface domain is discretized as a single layer of rectangular or triangular grid elements, while the subsurface domain is discretized as layers of either hexahedral blocks or triangular prisms. Linear features like channels, drains and wells are represented by 1-D linear elements. The surface and subsurface flow and transport domains are coupled either by using numerical superposition whereby the top layer of nodes represent both surface and subsurface domains, or by assuming the existence of a thin boundary layer between the surface nodes and the first layer of subsurface nodes across which the leakage of water (Darcy flux) and solutes (Fickian transport) occurs.

2.3 Control of Landscape Structure on Mountain Recharge, Groundwater Flow and Baseflow Generation

2.3.1 Synthetic Channel Network

We use synthetic channel networks with different geometrical and topological structures to explore the control of channel network structure on recharge and baseflow generation in mountainous watersheds. The synthetic channel networks are generated by using the optimum channel network (OCN) approach, which is based on two local and one global principles of minimizing stream energy expenditure (Rodríguez-Iturbe and Rinaldo, 1997). The two local principles require (i) minimum energy expenditure in any link of the stream network and (ii) equal energy expenditure per unit area of stream anywhere in the network, for transportation of a prescribed discharge throughout the basin. The global principle requires (iii) minimum energy expenditure in the stream network as a whole (Rodríguez-Iturbe and Rinaldo, 1997).

For site i in the channel network with stream link length L_i, elevation z_i and flow rate Q_i, the rate of potential energy loss (P_i) is:

$$P_i = \rho Q_i g L_i |\nabla z_i| \tag{2.17}$$

where ρ is the density of stream water, g is gravitational acceleration, and $|\nabla z_i|$ is the magnitude of the slope. The sediment discharge is ignored in Equation (2.17) because it's relatively small compared with the water discharge.

In the case of uniform rainfall input for long-term landscape evolution, it can be assumed that Q_i is proportional to the cumulative drainage area A_i, that is $Q_i \propto A_i$. Using the empirically observed scaling relationship between local topographic slope $|\nabla z_i|$ and cumulative drainage area A_i (Tarboton et al., 1989), which is

$$|\nabla z_i| = kA_i^\alpha \tag{2.18}$$

where $\alpha \in (-1,0)$ is the scaling exponent and k is the proportionality coefficient, equation (2.17) leads to $P_i \propto L_i A_i^{1+\alpha}$. Summing up the energy expenditure at all sites within the basin, we can get the total energy expenditure to be:

$$P = \sum_i P_i \propto \sum_i L_i A_i^{1+\alpha} \tag{2.19}$$

So the OCN characterized by minimum energy expenditure can be generated by searching for the channel network configuration s which minimizes the functional (Sun et al., 1994; Rinaldo et al., 2014):

$$H_\alpha(s) = \sum_i L_i A_i^{1+\alpha} \tag{2.20}$$

The exponent α is related to the mechanics of erosional processes in different climatic and physiographic regions (Rodríguez-Iturbe and Rinaldo, 1997), and is critical to the structure of the OCN (Hooshyar et al., 2017). α is varied to obtain channel networks with different structures.

The OCN is generated on a square grid with 352 rows times 285 columns. The size of the grid is determined by considering the limit of computational capacity, as well as the grid size used in previous studies (e.g., Sun et al., 1994; Rinaldo et al., 2014). The boundary of the basin is defined in a polar coordinate system as (Abed-Elmdoust et al., 2016)

$$r = L\exp(-\frac{L^2}{T^2}(\varphi - \varphi_0)^{2n}) \tag{2.21}$$

where r and φ are the radius and azimuth, and L and T represent the longitudinal and the transverse elongation of the basin. This shape is adopted to mimic a natural basin, and also the simple basin generated by a landscape elevation model (e.g. Perron et al., 2012). The total number of grid points within the basin is 32,560.

OCN with different structures are created by varying the value of α in equation (2.20). The α values

used are -0.999, -0.875, -0.75, -0.625, -0.5, -0.375, -0.25, -0.125, -0.001. For each α value, the seed for random number generation in the optimization process is changed for multiple simulations to get OCN scenarios with similar structure. We discard the networks whose Horton-Strahler orders differ from the most commonly occurring order of the networks. In our case, only networks of order 8 are retained and are used to generate associated DEM for groundwater simulation.

2.3.2 Topography Associated with the Synthetic Channel Network

Elevation fields associated with different OCN scenarios are needed for the hydrological simulations. Elevation is assigned to each site in the channel network by using equation (2.18) following the steps described below (Sun et al., 1994). Given the generated OCN and the corresponding flow direction, the cumulative drainage area at each site (A_i) can be calculated. Then the local topographic slope $|\nabla z_i|$ can be calculated by using equation (2.18). The elevation change from the upstream to the downstream direction along the surface flow path at each site can be calculated as

$$\delta h_i = |\nabla z_i| L_i \tag{2.22}$$

Assuming that the elevation of the outlet O is 0, the elevation of site i is calculated by summing the elevation changes across all sites along the flow pathway l_{iO} from site i with coordianates (x,y) to the outlet O

$$h_i(x,y) = \sum_{j \in l_{iO}} \delta h_j \tag{2.23}$$

The calculated elevation field associated with each channel network scenario is referred to as OCN-DEM.

2.3.3 Linearly and Exponentially Scaled OCN-DEM

The relief, slope of OCN-DEM and the longitudinal elevation profile of the streams are controlled by the k and α values in equation (2.18) (e.g. Peckham, 2015). The OCN-DEM's calculated using equation (2.23) preserve the distinct structures of channel network generated by optimizing equation (2.20) using different α values. However, since the magnitude of the slope is nonlinearly proportional to the cumulative drainage area A_i to an exponent α, α with small absolute values (e.g. -0.125) result in large local slope ($|\nabla z_i|$) and flank slope (defined as the slope from the highest peak to the lowest outlet point in the y direction, equation 2.24).

To separate partly the effect of different characteristics of topography (e.g., relief, local slope, flank slope) and channel network structure (e.g., geometry, topology), we scaled the OCN-DEM linearly and exponentially. The linear scaling maintains the planform structure of the channel network and the hypsometric curve of the DEM but constrains all the OCN-DEM to have the same flank slope, which is estimated here as:

$$\tan\beta = \frac{\max h(x,y) - \min h(x,y)}{L} \tag{2.24}$$

where β is the slope angle. We use $4°$, $10°$, $24°$ for the linearly scaled β, denoted as $\bar{\beta}$, to represent low relief, moderate relief, and high relief (Gleeson and Manning, 2008). Linearly scaled elevation is calculated as

$$\bar{h}(x,y) = h(x,y)\frac{L}{\max h(x,y) - \min h(x,y)}\tan\bar{\beta} \tag{2.25}$$

The exponential scaling is performed by using the same $\alpha = -0.5$ in equation (2.18) in the calculation of elevation associated with each OCN, regardless of what α value is used for the OCN generation. This processing might violate some geomorphological law, but it helps to fix the scaling relationship between slope and cumulative drainage area, and thus constrains the OCN-DEM's to have similar hypsometric curves while maintaining the planform structure of the channel network (Figure 3.9). This processing helps to separate out the effect of channel network structure and fits our study purpose.

2.3.4 Soil Zone Thickness Associated with Topography Scenarios

Including the soil zone in geology scenarios is important because the soil zone typically has higher hydraulic conductivity, caused by root tunnels and animal burrows, than the underlying bedrock, and provides a fast flow path for water and dissolved solutes (e.g., Beven and Germann, 1982, 2013). In addition, the soil zone thickness is related to the bedrock topography, which determines the threshold precipitation amount for the fill and spill of bedrock depressions, the connectivity of subsurface saturated areas, and the nonlinear increase of subsurface runoff during storm events (e.g., Tromp-van Meerveld and McDonnell, 2006).

We estimate the soil zone thickness using the simple analytical method of Liu et al. (2013). This method is based on the dynamic equilibrium between soil production and transport. The soil production rate is assumed to decrease exponentially with increasing soil thickness. The soil transport flux is determined by

the local topographic slope for soil flux driven by soil creep, and by slope and cumulative drainage area for soil flux driven by fluvial transport. The method is limited to humid and semi-arid regions where subsurface storm flow instead of infiltration-excess overland flow dominates the runoff component, and the bedrock is mechanically strong. It also assumes no tectonic uplift or base level lowering during the period of landscape evolution. These assumptions are consistent with our model scenarios and thus make this method suitable for our purpose of estimating soil zone thickness. This method only requires the elevation data and has been tested using field observations. The details of implementing the method can be found in (Liu et al., 2013).

2.3.5 Width-Function-Based GUH

We use width-function-based geomorphological unit hydrograph (WFGUH) to measure the effect of channel network structure on surface runoff routing. The width function, denoted by $W(x)$, is the area of the watershed at the same distance from the outlet, as measured along the streams and the drainage paths (e.g., Rigon et al., 2016). Assuming that all water parcels flow at the same constant celerity, u_c, the probability density function of the travel time can be calculated as:

$$p_w(t - t_i) = \int_0^S w(x) f(t - t_i|x) dx \tag{2.26}$$

where S is the length of the main stream, $w(x)$ is the normalized width function, and $f(t - t_i|x)$ is the travel time distribution conditioned on the distance x to the outlet, which can be approximated as:

$$f(t|x) = \frac{x}{\sqrt{4\pi D t^3}} \exp\left[-\frac{(x - u_c t)^2}{4Dt}\right] \tag{2.27}$$

where D is the diffusion coefficient characterizing the diffusive processes as in (Rinaldo et al., 1991).

Assuming that the runoff rate at time t_i is $J(t_i)$ and all the parameters are spatially and temporally constant, the WFGUH can be expressed as:

$$Q(t) = \int_0^t J(t_i) \int_0^S \frac{xw(x)}{\sqrt{4\pi D(t - t_i)^3}} \exp\left[-\frac{(x - u_c(t - t_i))^2}{4D(t - t_i)}\right] dx dt_i \tag{2.28}$$

2.3.6 Drainage Experiment using MODFLOW

We use MODFLOW (Harbaugh, 2005) developed by the US Geological Survey to simulate groundwater drainage processes in the synthetic watersheds to investigate the controlling mechanism of topographic and channel network structure on baseflow recession. A drain boundary condition is applied to the top boundary corresponding to the land surface to simulate head-dependent drainage flux. Water drains out of the watershed when the hydraulic head at the top layer is higher than the land surface elevation. The drain flux is calculated as the product of the difference between hydraulic head and land surface elevation and the drain conductance C_D. No water flows out of the watershed if the hydraulic head at the top layer is lower than the land surface. Lateral and bottom boundaries are assumed to be impervious. The mathematical statement under these assumptions is given by

$$\nabla \cdot [K\nabla h] + W = S_s \frac{\partial h}{\partial t} \tag{2.29}$$

$$q(x, y, z = z_0(x, y)) = C_D(h - z_0) \quad \text{,if} \quad h > z_0 \quad \text{on} \quad \partial\Omega_1 \tag{2.30}$$

$$q(x, y, z = z_0(x, y)) = 0 \quad \text{,if} \quad h \leq z_0 \quad \text{on} \quad \partial\Omega_1 \tag{2.31}$$

$$\vec{n} \cdot [K\nabla h] = 0 \quad \text{on} \quad \partial\Omega_2 \text{ and } \partial\Omega_3 \tag{2.32}$$

where h is hydraulic head [L], K is hydraulic conductivity [LT^{-1}], W is a volumetric flux per unit volume representing sources and/or sinks of water [T^{-1}], S_s is the specific storage of the porous material [L^{-1}], t is time [T], q is flow rate draining from the aquifer through the land surface [L^{3}T^{-1}], C_D is the drain conductance [L^{2}T^{-1}], z_0 is land surface elevation [L], $\vec{n}$ is the outward normal vector at the boundary, $\partial\Omega_1$ is the top boundary, $\partial\Omega_2$ is the lateral boundary, and $\partial\Omega_3$ is the bottom boundary.

The initial condition for the drainage is taken as the steady-state solution of the groundwater flow problem with land surface elevation as specified hydraulic head top boundary condition and no lateral and bottom flux boundary conditions, as shown by the following mathematical statement

$$\nabla \cdot [K\nabla h] = 0 \tag{2.33}$$

$$h(x, y, z = z_0(x, y)) = z_0(x, y) \quad \text{on} \quad \partial\Omega_1 \tag{2.34}$$

$$\vec{n} \cdot [K\nabla h] = 0 \quad \text{on} \quad \partial\Omega_2 \text{ and } \partial\Omega_3 \tag{2.35}$$

Chapter 3

DISCUSSION OF RESULTS AND THEIR SIGNIFICANCE

3.1 The Importance of Capturing Topographic Features for Recharge Modeling in Complex Mountainous Terrains

We use HGS to explore the importance of topography in hydrological processes within mountainous watersheds. In particular, we explored the effect of topographic features such as streams and ridges on the simulated internal groundwater flow and transport patterns and recharge to mountain front aquifers under different geological heterogeneity scenarios. A key part of this analysis is the use of different meshes, that vary in their fidelity and ability to capture topographic features (i.e., topographic complexity level; TCL) and allow us to evaluate the implications of mesh characteristics in the model results – a theoretical contribution with fundamental implications for applied modeling studies.

Examples of the simulated heads and groundwater ages for the Rio Hondo watershed are shown in figures 3.1a and 3.1b). Similar models were generated for different topographic complexity levels (i.e., different meshes) and subsurface heterogeneities, resulting in 56 models.

We use these models to explore the importance of generating meshes that capture key topographic features and its implications for mountain recharge, runoff generation, residence times, and solute transport. We find that capturing the river network structure is fundamental to reproduce appropriately the nested network of flow paths observed in mountainous terrains. Due to computational limitations, these features are
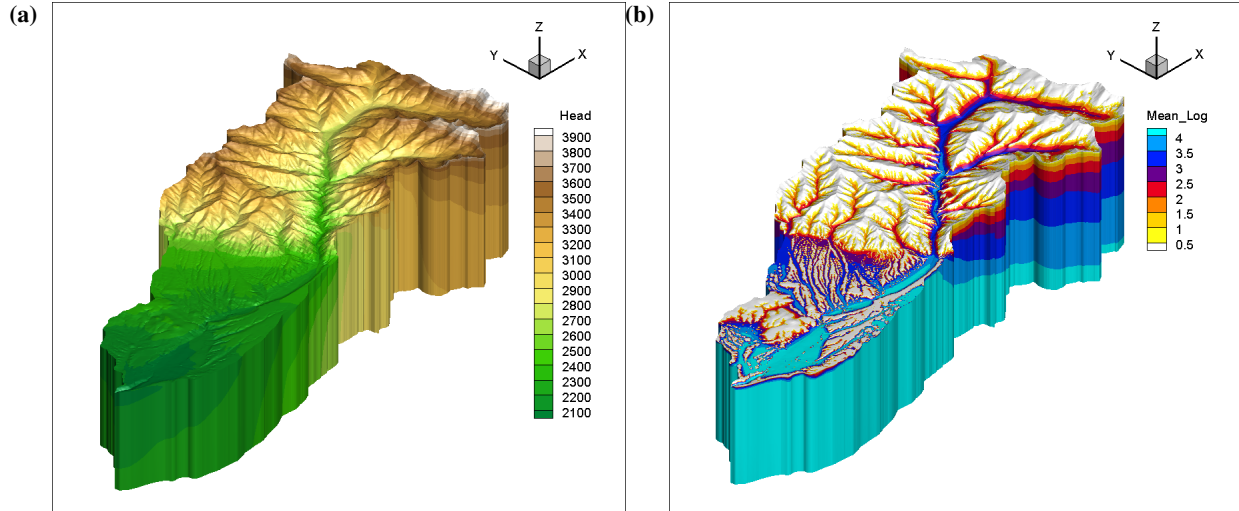
Figure 3.1: Simulated steady-state groundwater (a) head (unit: m) and (b) mean age (unit: day) in Rio Hondo watershed under fully-saturated conditions.

typically oversimplified in modeling efforts, resulting in misguided interpretations of observations and biased assessments of water resources, solutes, and contaminants. Our findings have fundamental implications for the interpretation of models in water resources assessments, the use and interpretation of environmental tracers, and the estimation of weathering rates. We describe in detail our findings in the following subsections.

3.1.1 The Effect of Capturing Streams by the Mesh

Net Flux Generated within the Domain

Table 3.1 summarizes the net baseflow generated within the simulation domain. For each K scenario, the net baseflow increases as the mesh is refined along more stream or ridge features. Refined mesh better captures the thalweg of the streams or the peak of the ridges, thus increasing the gradient of hydraulic head along flow paths, and thus increasing groundwater flow rate and baseflow into streams. Refining the mesh along more streams or ridges also enables the model to capture more local scale undulations of the water table along streams or ridges, which drive more local scale flow paths to be formed and thus increase the net baseflow.

Decreasing extinction-depth of K enhances the effect of model TCL on the net baseflow within the simulation domain. The change of net baseflow within the whole domain caused by mesh TCL is less than 10% for models using extinction-depth of at least 33.3 m (Table 3.1). This indicates that for watersheds with fractured and permeable bedrock that has relatively deep extinction-depth, the effect of mesh TCL on

Table 3.1: Total baseflow generated within the modelling domain from models using exponentially decaying hydraulic conductivity with different extinction-depths, and meshes of different topographic complexity levels (TCLs) (Unit: m^3/s)

| TCL	∞	1000 m	333.3 m	100 m	33.3 m	10 m	3.3 m
1S	2218	1979	1685	1190	698	296	110
1SR	2225	1986	1692	1197	704	301	112
2S	2224	1985	1693	1198	706	302	113
2SR	2239	2000	1707	1212	719	311	117
3S	2235	1997	1705	1212	720	312	117
3SR	2273	2035	1742	1247	750	332	128
4S	2253	2016	1724	1230	735	321	122
4SR	2298	2061	1769	1273	774	349	136
Max. Diff. [a] (%)	3.5	4.0	4.7	6.5	9.8	15	19

[a]Max. Diff. is the maximum relative difference of total baseflow from models with different mesh TCLs but using the same hydraulic conductivity field.

net groundwater discharge in the simulation domain can be relatively small. But for watersheds where the permeability of the bedrock decreases relatively fast with depth, the effect of mesh TCL on net groundwater discharge within the domain can be significant.

Flushing Intensity of Groundwater Flow

Not refining the mesh along some of the streams (TCL1S, TCL2S, TCL3S) causes negative bias of flushing intensity, as compared to the model with mesh refined along all streams (TCL4S). This is consistent for all K scenarios (Fig. 3.2). In addition, the less lower-order streams are captured in the mesh (TCL3S, TCL2S, TCL1S), the larger is the magnitude of the bias of flushing intensity. The bias of flushing intensity is mostly found within the top 500 m of the modeling domain. The largest bias is found at the top of the domain, but the magnitude is less than 2%. The magnitude of flushing intensity decreases with depth.

Heterogeneity of K can influence the effect of TCL on flushing intensity. When the extinction-depth is deeper than 10 m (Fig. 3.2 (a)-(e)), decreasing extinction-depth enhances the bias of flushing intensity caused by mesh TCL, and most of the enhancement occurs above the extinction-depth (Fig. 3.2). This is because shallow extinction-depth suppresses the development of the deep intermediate and regional groundwater flow paths and enhances groundwater circulation along the shallow local flow paths (Cardenas and Jiang, 2010). The shallow local flow paths can be affected more by capturing local water table undulations than the deep regional flow paths. However, as the extinction-depth further decreases (Fig. 3.2 (f)-(g)), the bias of flushing intensity above the extinction-depth becomes smaller, but the bias below the extinction-depth becomes larger.
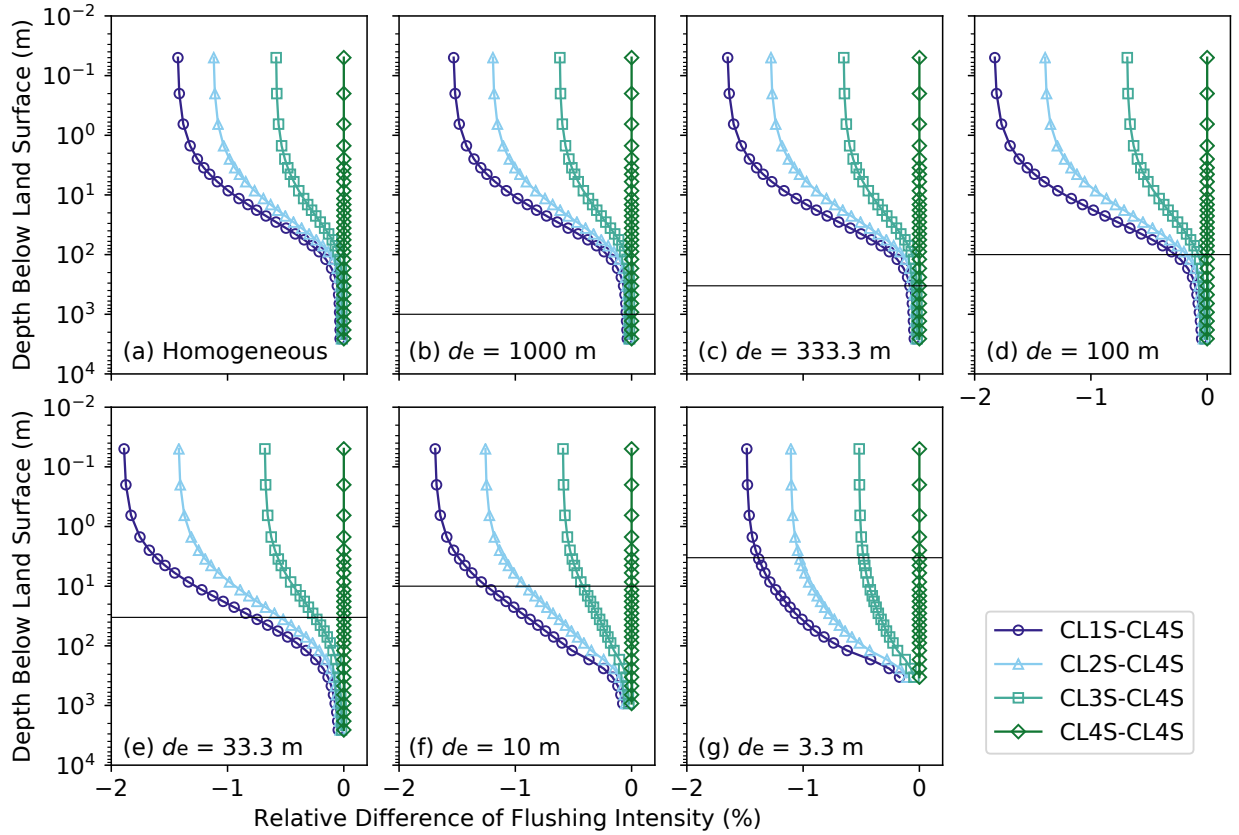
Figure 3.2: Effect of capturing different amount of stream topographic features on the flushing intensity of simulated groundwater flow, and the influence of geological heterogeneity. Flushing intensity of groundwater flow from models with meshes refined along different amount of streams (TCL1S, TCL2S, TCL3S) is compared to the result from the model with mesh refined along all the stream features (TCL4S). Different subplots show results from simulations using hydraulic conductivity fields with different extinction-depths, as marked by the solid horizontal lines.

## Groundwater Circulation and Baseflow Generation

In addition to the effect of mesh TCL on the lumped metrics including flushing intensity of groundwater flow through vertical layers and the net flux of baseflow generated within the simulation domain, significant and different effects can be found for baseflow into streams of different orders (Fig. 3.3), further reflecting the effect of mesh TCL on the nesting and spatial distribution of the groundwater flow paths. The results from models with TCLiclS ($icl = 1, 2, 3$) are evaluated against results from the model with TCL4S, following the approach described in the Methods section. Generally, for models with mesh capturing fewer stream features, baseflow into higher-order streams ($\omega = 3, 4, 5$) is dominated by positive bias, while baseflow into lower-order streams ($\omega = 1, 2$) is dominated by negative bias. This is because models with meshes refined along more stream features better capture topographic variability at the local scale (e.g., stream bank and channel), and therefore are able to capture high-frequency spatial variations in the water table that ultimately

21

drives water through local scale flow paths and generates more baseflow in lower-order streams. Meanwhile, flow through intermediate and regional flow paths is reduced, resulting in less baseflow into the higher-order streams.

Specifically, for the fifth-order stream, baseflow is biased higher in models with TCL*icl*S ($icl = 1, 2, 3$) as compared to the model with TCL4S. As more streams of order lower than 5 are captured by the model (from TCL1S to TCL4S), the positive bias of baseflow into the fifth-order stream decreases, which indicates that capturing lower-order streams besides the main stream can have a significant effect on simulated baseflow into the main stream. Similar effects can be found for fourth-order streams. For third-order streams, when they are not captured by the model (TCL1S), baseflow into these streams is biased lower. Once they are captured by the model (TCL2S and TCL3S), baseflow into these streams is biased higher, and the interquantile range (IQR) of the bias is smaller. The median bias decreases from the model with TCL2S to the model with TCL3S, as TCL3S further captures second-order streams more than TCL2S. Following the same thread, baseflow into second-order streams is biased lower when second-order streams are not captured by the model (TCL1S and TCL2S), and is biased higher with smaller IQR of the bias when second-order streams are captured by the model (TCL3S).

These bias effects of capturing stream features are consistent for all K scenarios but are more obvious with shallower extinction-depth of K (Fig. 3.3 columns from left to right). These detailed effects can be summarized by noting that, if streams of order ω were not captured in the model with TCL*icl*S, then baseflow into streams of order ω from the model with TCL*icl*S will be less than baseflow into streams of order ω from models with meshes that capture streams of order ω. And the more streams of order other than ω are captured in model with TCL*icl*S, the less baseflow flows into streams of order ω. On the other hand, if streams of order ω are captured in the model, then the less streams of order other than ω are captured simultaneously, and the more baseflow flows into streams of order ω. So refining the mesh along streams makes the streams more 'competitive' in draining groundwater to generate baseflow. And refining the mesh along streams of certain order not only affects the baseflow into streams of that order, but also affects the subsurface flow paths across all scales and baseflow into streams of other orders.

For first-order streams, the magnitude of median bias is relatively small, especially for models using K with extinction-depths deeper than 33.3 m. When more streams other than first-order are captured by the mesh, less and less groundwater discharges into first-order streams. This is consistent with the effect of mesh TCL on baseflow into second- to fifth-order streams, as described above. However, the bias changes from negative to positive as the extinction-depth of K decreases (first row in Fig. 3.3). In models with relatively
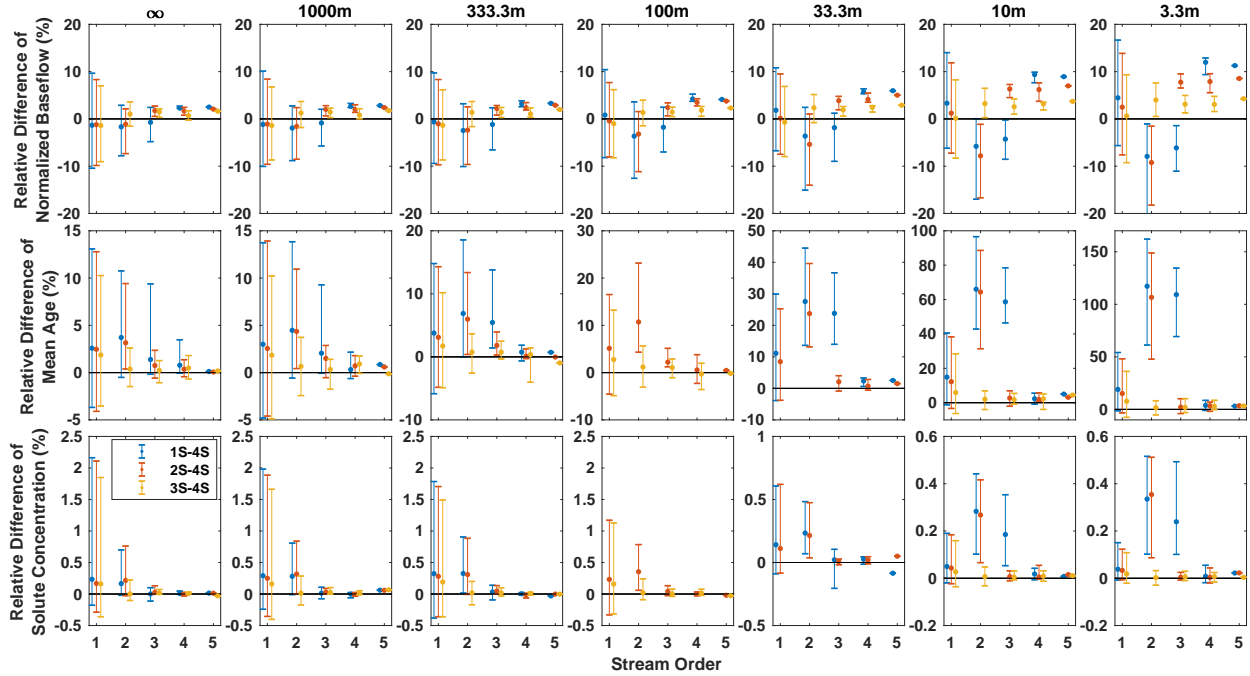
Figure 3.3: Effect of capturing different amounts of stream topographic features on the normalized flow rate, mean age, and solute concentration (SiO_2 as an example, from subsurface chemical weathering) of baseflow into streams of different orders, and the influence of geological heterogeneity. The relative difference of each metric is calculated in the way described in the Methods section. Results from models with meshes capturing different amounts of stream features (TCL1S, TCL2S, TCL3S) are compared to the result from the model with mesh capturing all the stream features (TCL4S). The median value (dots) and interquantile range (IQR, error bars) of relative differences for streams of each order are plotted. Different columns show results from the simulations using exponentially decaying hydraulic conductivity fields with different extinction depths, as indicated by the column label at the top.

deep extinction-depth, baseflow into first-order streams is biased lower when first-order streams are not captured by the mesh. This is consistent with our explanation that not capturing local-scale topographic variability along these first-order streams smooths the local scale water table undulation and drives less water through these local scale short flow paths into first-order streams. However, for models using K with extinction-depth shallower than 10 m, not capturing first-order streams (TCL1S, TCL2S, TCL3S) results in positive bias of baseflow into first-order streams, as compared to the model with mesh capturing first-order streams (TCL4S).

The IQR of the bias of baseflow is also affected by the model TCL. Generally, the IQR of the bias decreases as more topographic features are captured by the mesh. The IQR of the bias for streams of order ω decreases significantly when the streams of order ω are captured by the mesh. Narrower IQR means that the bias for different streams get closer to the median bias. Changes of IQR of the bias indicate that different streams of the same order have different sensitivity to model TCL in terms of gaining baseflow. The IQR of the bias is also larger for lower order streams. This is because of more stream links of lower-order on

23

one aspect, and lower-order streams gaining water from shallower flow paths that can be influenced more by capturing topographic variability, on the other aspect.

Regarding the influence of the extinction-depth of K on the effect of model TCL, we find that decreasing extinction-depth of K enhances the bias effect of model TCL, in terms of increasing of the magnitude of the median bias, increasing of the differences of the bias among model TCLs, and increasing of the IQR of the bias. This is because decreasing the extinction-depth enhances the shallow circulation by forcing more water into shallow and local flow paths (Cardenas and Jiang, 2010), and the shallow groundwater circulation can be affected more by capturing local topographic variability.

The bias effect of missing streams on baseflow generation can be more important if the model is coupled with ecological processes and simulates evapotranspiration. Spatial distribution of stream flow generation can influence riparian plant distribution. Models with low TCL generate more water into the main stream and could make more plants concentrate along the main stream riparian zone with fewer plants along tributaries and influence the spatial distribution of evapotranspiration and further bias the simulated stream flow spatial distribution and water balance.

Baseflow Mean Age

Generally, the mean age of baseflow from models with meshes capturing less lower-order streams is biased older for streams of all orders. Capturing streams of order ω can significantly reduce the mean age of baseflow into streams of order ω (Fig. 3.3). This is consistent with the effect of mesh TCL on the normalized flow rate. Capturing more local scale high-frequency topographic features through mesh refinement drives relatively more water to flow through shorter and shallower local-scale subsurface flow paths and relatively less water to flow through longer and deeper regional scale flow paths. This leads to more young water flowing into lower-order streams and less old water flowing into higher-order streams, which means that baseflow mean age from models with high TCL is predominantly younger than that from models with low TCL.

For the first-order streams, mean age of baseflow from models with TCL1S, TCL2S and TCL3S is predominantly biased older than that from the model with TCL4S (Fig. 3.3). Comparing TCL1S, TCL2S and TCL3S to TCL4S, we find that the most significant bias is caused by not refining the mesh along first-order streams (from TCL4S to TCL3S), which means that refining the mesh along first-order streams, which are typically ignored in the modeling practice, can be important to reproduce the mean age of baseflow into

24

these headwater streams. Further missing streams higher than order 1 (TCL3S, TCL2S, TCL1S) gradually leads to older and older baseflow, but the increase of bias is not as significant as that caused by missing first-order streams (from TCL4S to TCL3S). The IQR of the bias also increases from TCL3S to TCL1S, indicating that mean age of baseflow into first-order streams can also be affected by not refining the mesh along higher-order streams, which leads to more extreme bias in some stream links. This can be informative for interpreting the modeling results since it tells us that some stream links may have bias extremely higher or lower than the median bias, which deserves some caution depending on the modeling purpose. These bias patterns are consistent for K with different extinction-depths, but the magnitude of the median value and the IQR of the bias both increase as the extinction-depth decreases.

For second-order streams, the effect of mesh TCL on baseflow mean age is similar to that for first-order streams. Briefly speaking, capturing more lower-order streams from TCL1S to TCL3S decreases the median value and the IQR of the bias. And the most significant decrease of the median value and the IQR of the bias is caused by refining the mesh along second-order streams (from TCL2S to TCL3S). Missing first-order streams doesn't cause much bias of mean age for second-order streams (from TCL3S to TCL4S). The bias effect is similar for different K scenarios but is enhanced under K with shallow extinction-depth. Similar results can be found for third- and fourth-order streams.

For the fifth-order stream, the bias of baseflow mean age caused by mesh TCL is within 5% for all K scenarios, but increases as the extinction-depth of K decreases. For the model using homogeneous K, there is little bias caused by mesh TCL. As the extinction-depth of K decreases but remains deeper than 3.3 m, missing more and more lower-order streams (TCL3S, TCL2S, TCL1S) biases the baseflow older and older. But as the extinction-depth of K gets too shallow (3.3 m), missing streams higher than order 1 has no significant impact on the mean age (TCL1S, TCL2S, TCL3S), and the bias is mainly caused by missing the first-order streams (from TCL4S to TCL3S). The groundwater circulation system in the model with shallow extinction-depth for K has mainly shallow and local flow paths developed (Cardenas and Jiang, 2010) and the intermediate and regional flow paths are suppressed. This kind of groundwater circulation system is more sensitive to capturing first-order streams than to capturing higher-order streams. These indicate that for the modeling in watersheds with bedrock permeability decreasing rapidly with depth, baseflow into the main stream (fifth-order in this study) might not be sensitive to mesh refinement along streams higher than order 1, but could be sensitive to mesh refinement along streams of order 1. The common modeling practice in which the mesh is refined along only high-order streams can lead to significant bias of the mean age of baseflow into the main stream. Therefore, the modeler should be more cautious with respect to the effect of

mesh resolution along headwater streams for watersheds dominated by shallow flow systems.

The effect of model TCL on baseflow mean age has similar patterns under K with different extinction-depths. Capturing detailed local topographic variability affects baseflow mean age more for models with shallower extinction-depths of K (Fig. 3.3). This is revealed in both the magnitude of the median value and the IQR of the bias. For baseflow mean age from models with shallower extinction-depth, the magnitude of the median value and the IQR of the bias caused by mesh TCL is larger. In this case, K with shallower extinction-depth forces groundwater to predominantly flow through the upper part of the modeling domain (Cardenas and Jiang, 2010), and the effects of capturing local topographic variability on the spatial distribution of groundwater discharge are enhanced. This is also consistent with the observation in the field that in watersheds with shallow and relatively impermeable bedrock and dominated by shallow flow paths, catchment mean transit time is more correlated to topographic indices, including median flow path gradient and median path length, than in watersheds with fractured permeable bedrock (Hale and McDonnell, 2016a). Furthermore, the influence of heterogeneity of K gets abruptly more pronounced when the extinction-depth is not deeper than 33.3 m, and the mean age of baseflow into streams of order 1 to 3 are the most sensitive to mesh TCL (Figure 3.3). This indicates the mean age of baseflow in lower-order streams in watersheds with bedrock that has shallow extinction-depth is the most sensitive to capturing stream features in the mesh.

Solute Concentration of Baseflow

The concentration of solute (SiO_2 as an example in this study) from subsurface chemical weathering is a function of the Damköhler number (Equation 2.15), which is proportional to groundwater residence time (Equation 2.16). As groundwater residence time approaches chemical equilibrium time, solute concentration approaches equilibrium concentration (Equation 2.15). The effect of mesh TCL on baseflow solute concentration is consistent with that on baseflow mean age, that is, solute concentration is biased higher when mean age is biased older due to less lower-order streams being used to refine the mesh. But for higher-order streams that get very old baseflow, the bias effect of mesh TCL is diminished due to the constraint of chemical equilibrium concentration.

For first-order streams, low TCL results in longer groundwater residence time and reaction time and thus higher solute concentration. The effect of mesh TCL is most significant when the mesh is not refined along first-order streams (from TCL4S to TCL3S). Similar effects can be found for second-order streams. The median bias is within 1%, and the IQR of the bias is within 2%, which means that the simulated baseflow solute concentration is less sensitive to mesh TCL than the flow rate and mean age.

Solute concentration in lower-order streams ($\omega = 1, 2$) from models with deeper extinction-depth (e.g., the homogeneous K) is affected more by mesh TCL, in terms of the median value and the IQR of the bias, as compared to models with shallower extinction-depth.

Simulated solute concentration is less affected by mesh TCL in models with shallow extinction-depth (Fig. 3.3), because baseflow generated by these models is relatively old and the chemical weathering is closer to equilibrium before the groundwater discharges into streams. The higher order streams ($\omega = 3, 4, 5$) also have an unbiased median concentration when the model TCL changes, because higher order streams gain water from longer regional flow paths with relatively long residence time during which the chemical weathering reaches equilibrium before the groundwater discharges into streams.

### 3.1.2 The Effect of Refining the Mesh along Ridges

Groundwater Flushing Intensity

If the mesh is refined along streams of certain orders, but the ridges of corresponding orders are not used for mesh refinement, then negative bias of flushing intensity can be found along the depth (Fig. 3.4). And the more ridges are missed in the mesh, the larger is the magnitude of the bias (from TCL4S to TCL1S). The magnitude of the bias is largest at the top of the modelling domain and decreases with depth, but the magnitude is less than 2%. The pattern of the bias is consistent under different K conditions, but the magnitude of the bias above the extinction-depth is enhanced when the extinction-depth decreases but is not shallower than 33.3 m (Fig. 3.4 (a)-(e)). The magnitude of the bias decreases above the extinction-depth and increases below the extinction-depth, when the extinction-depth further decreases to shallower than 10 m (Fig. 3.4 (f)-(g)).

If only high-order streams are used for mesh refinement, then the bias caused by not refining the mesh along corresponding high-order ridges is relatively small (TCL1S vs TCL1SR). However, when streams of all orders are used for mesh refinement, the bias caused by not refining the mesh along corresponding ridges is largest.

Groundwater Circulation and Baseflow Generation

Not refining the mesh along the ridges corresponding to the order of streams used for mesh refinement leads to negative bias of baseflow for first-order streams, and positive bias for streams higher than order 1 (Fig.

27
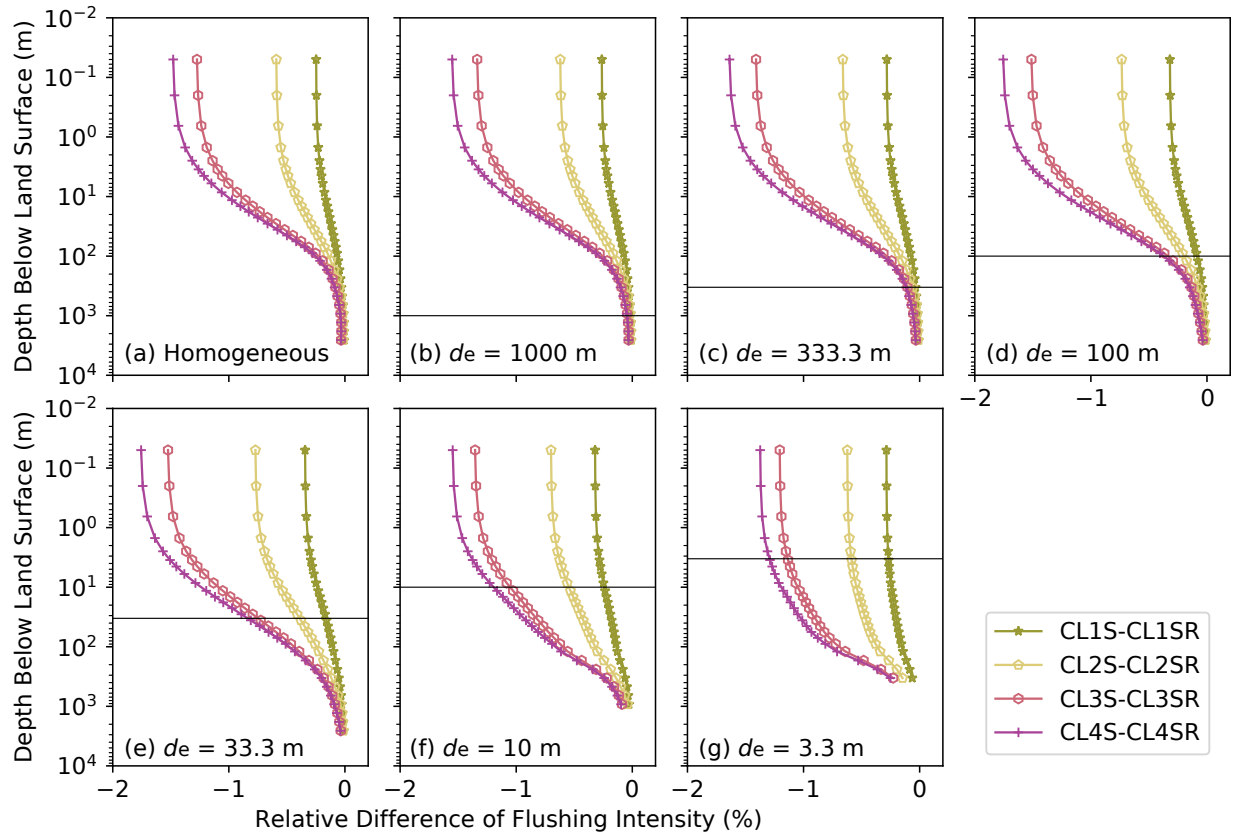
Figure 3.4: Effect of capturing ridges in addition to capturing streams on the flushing intensity of simulated groundwater flow, and the influence of geological heterogeneity. Flushing intensity of groundwater flow from models with meshes capturing only stream features (TCL1S, TCL2S, TCL3S, TCL4S) is compared to that from models with meshes capturing streams as well as ridges of the corresponding order (TCL1SR, TCL2SR, TCL3SR, TCL4SR). Different subplots show results from simulations using hydraulic conductivity fields with different extinction-depths, as marked by the solid horizontal lines.

3.5). Decreasing extinction-depth increases both the magnitude of the median bias, and the IQR of the bias, which is consistent with the effect of mesh TCL on the flushing intensity.

In more detail, for first-order streams, the bias effect is more significant when first- and second-order ridges are not captured by the mesh (TCL3S vs TCL3SR, and TCL4S vs TCL4SR). For second-order streams, when the extinction-depth is not shallower than 333.3 m, the bias is most significant when fourth- and fifth-order ridges are not used for mesh refinement (TCL1S vs TCL1SR). But when the extinction-depth is shallower than 333.3 m, the bias is more significant when more lower-order ridges are not used for mesh refinement (e.g., TCL4S vs TCL4SR). For third-order streams, bias is minimal between the model TCL2S and TCL2SR, which means that when streams of order 5,4 and 3 are used for mesh refinement, the bias caused by not refining the mesh along corresponding ridges is small. For fourth- and fifth-order streams, the bias increases as the mesh captures more streams but no corresponding ridges (from TCL1S to TCL4S, compared to TCL1SR to TCL4SR, respectively).
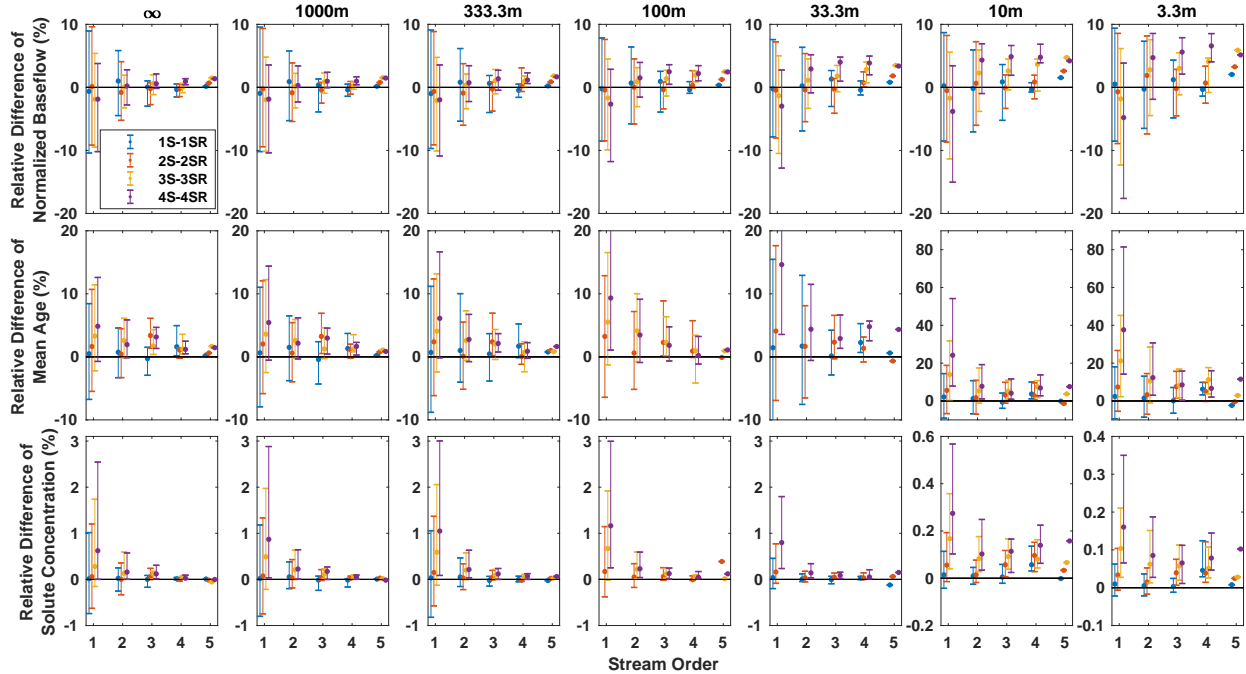
Figure 3.5: Effect of capturing ridges in addition to capturing streams on the normalized flow rate, mean age, and solute (SiO_2 as an example, from subsurface chemical weathering) concentration of baseflow into streams of different orders, and the influence of geological heterogeneity. Results from models with meshes capturing only stream features (TCL1S, TCL2S, TCL3S, TCL4S) are compared to the results from models with meshes capturing streams as well as ridges of the corresponding order (TCL1SR, TCL2SR, TCL3SR, TCL4SR). Different columns show results from simulations using hydraulic conductivity fields with different extinction-depths, as indicated by the column label at the top.

Generally, ridges become important when corresponding streams are used for mesh refinement. The bias caused by not refining the mesh along the ridges is relatively small when only high-order streams are used for mesh refinement (e.g., TCL1S vs TCL1SR). However, if lower-order streams are needed for mesh refinement in order to reduce the bias of simulated hydrological variables (Fig. 3.3), then the mesh must also be refined along lower-order ridges to reduce the bias. Otherwise, the mesh capturing all the streams (TCL4S), which is used as a benchmark to evaluate the effect of missing streams, leads to large bias compared to the model with mesh capturing both the streams and ridges (TCL4SR). Although it might not be possible to refine the mesh along all streams and ridges due to the limit of computational capacity, the bias effect of missing these topographic features must be taken into account when interpreting the modelling results.

Baseflow Mean Age

Capturing only streams but no ridges in the mesh biases the baseflow mean age older. This is consistent with the bias effect on baseflow flow rate, as missing more lower-order ridges smooths the local scale water table

variability and causes more water to flow through longer regional flow paths and less water to flow through shorter local flow paths.

For first-order streams, baseflow is biased older and older when more and more streams are captured by the mesh but no corresponding ridges are captured. For second-order streams, the most significant bias occurs when second-order streams are captured in the mesh but no ridges are captured (TCL3S vs TCL3SR). Similar effect can be found for third-order streams, that is, when all the third-order streams but no third-order ridges are captured by the mesh, the bias is the most significant. For fifth-order streams, the bias gets larger when more ridges are not captured by the mesh.

The effect of mesh TCL on baseflow mean age is consistent under different K conditions, but the effect is enhanced in terms of the magnitude of the median bias value and the IQR of the bias, as the extinction-depth decreases.
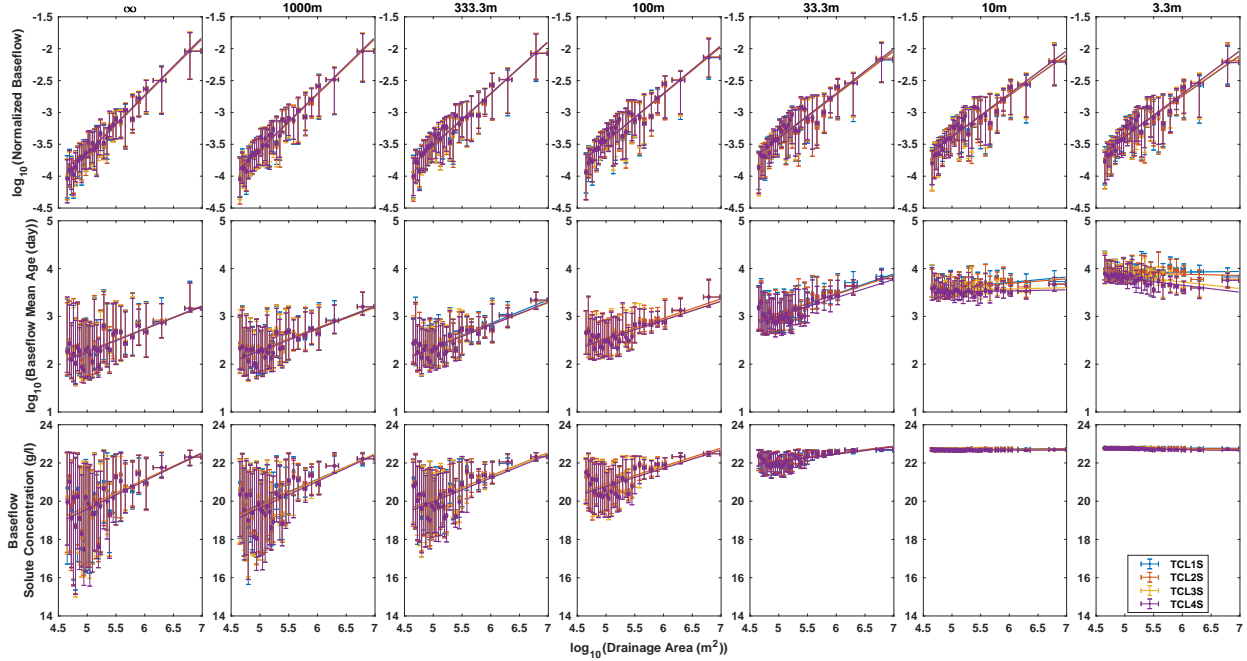
Baseflow Solute Concentration

The effect of not capturing ridges on baseflow solute concentration is consistent with that on baseflow mean age, since baseflow solution concentration is directly a function of baseflow mean age (Equation 2.15). The effect is more significant for lower-order streams and for models using K with shallower extinction-depths. But the overall bias is within 3%, which means baseflow solute concentration is not as sensitive to capturing ridges in the mesh as the flow rate and mean age, especially for higher-order streams and for watersheds with rapidly depth-decaying K and dominated by old baseflow.

3.1.3   The Effect of Mesh TCL on Baseflow Spatial Scaling

Previous work has found a general spatial scaling pattern between groundwater contribution to streamflow and drainage area (Frisbee et al., 2011). These patterns are explained well by a 3-D catchment-mixing conceptual model with a topography-driven nested groundwater flow system. Our ideal model with the topography-driven groundwater flow assumption reproduces these findings from natural watersheds (Frisbee et al., 2011) and shows strong power-law scaling between flow rate, mean age, solute concentration of baseflow and drainage area (Figs. 3.6 and 3.7).

The spatial scaling between baseflow and drainage area is affected little by the mesh TCL for models using extinction-depths deeper than 10 m, and affected slightly by mesh TCL for models using extinction-depths of 10 m and 3 m in which case the scaling slope decreases slightly with lower mesh TCL (Fig. 3.6 and

Figure 3.6: Change of binned normalized flow rate, mean age, and solute concentration of baseflow with binned drainage area from models with meshes capturing streams only.

3.7). This indicates that capturing local scale topographic variability along streams or ridges has a very small effect on this lumped spatial scaling metric. But as extinction-depth decreases, the intermediate and regional scale groundwater flow paths are suppressed and the local scale circulation is enhanced (Cardenas and Jiang, 2010), and this leads to a slightly decreasing of the scaling slope with the decreasing of extinction-depth.

For baseflow mean age and solute concentration (Fig. 3.6 and 3.7), the binned values are more scattered around the fitted trend. This indicates that the transport process and stream water chemistry are affected more by multi-scale topographic variability and bio-geo-chemical processes (e.g. McGuire et al., 2014). Little effect of mesh TCL on the scaling slope of solute concentration can be found. The scaling slope of mean age is affected slightly for models using extinction-depths of 10 m and 3.3 m. The scaling slope of baseflow mean age decreases and approaches 0 as extinction-depth decreases. This is because although the regional scale flow paths are suppressed in models with shallow extinction-depth, the very old water from the part of the modelling domain with low K, although of small amount, still controls the baseflow mean age and makes the baseflow very old. This is why the baseflow is very old even for small drainage areas (e.g. last plot in the second row of Fig. 3.6). And the very long mean age leads to relatively stable solute concentrations for streams with large drainage areas and for models with shallow extinction-depths of K.
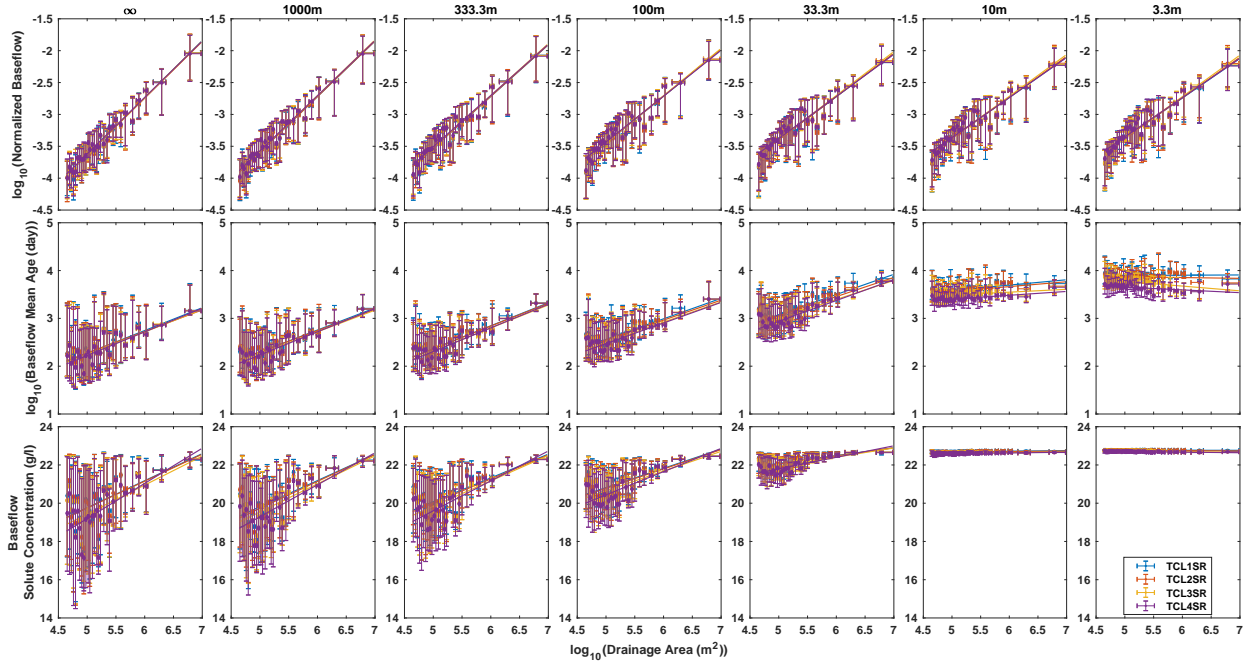
Figure 3.7: Change of binned normalized flow rate, mean age, and solute concentration of baseflow with binned drainage area from models with meshes capturing streams and ridges.

3.1.4 Summary

Mesh TCL has a relatively small influence on the integrated metrics including net flux, flushing intensity, and spatial scaling of flow rate, mean age and solute concentration. However, mesh TCL can significantly affect the relative amount of groundwater through subsurface flow paths of different scales and the relative amount of baseflow into streams of different orders. When compared to the model with the highest TCL, lower TCL models capturing less topographic features, such as low-order streams or ridges, produce less flow through short, local scale flow paths and more flow through longer, intermediate and regional scale flow paths. This results in less baseflow into low-order streams and more baseflow into high-order streams.

Meshes that ignore low-order streams and ridges can reduce flow through shallow and short local scale flow paths and increase flow through deep and long regional scale flow paths. This results in lower amount of young water flowing into low-order streams and larger amount of old water flowing into high-order streams. The overall effect is that the baseflow into streams of all orders is biased older in models with low TCL than the models with high TCL which capture more stream or ridge features.

Baseflow solute concentration is less sensitive to model TCL due to the constraint of thermodynamic limit on equilibrium concentration. In models with rapidly decaying hydraulic conductivity or for high-order streams, the mean age of groundwater discharging into streams are longer than equilibrium time of

chemical reaction. So in these cases the solute concentration approaches equilibrium concentration and is affected little by mesh TCL. For low-order streams in models with slowly decaying hydraulic conductivity, the mean age of groundwater discharging into streams is shorter than chemical equilibrium time and the change of mean age caused by mesh TCL can affect solute concentration in these low-order streams.

A shallower extinction depth of hydraulic conductivity enhances the effect of mesh TCL on flow rate and mean age of baseflow, because the subsurface flow system is forced at the upper part of the modeling domain and is affected more by capturing local water table variability. The effect of mesh TCL should be more significant in models of regions with shallow and low permeability bedrock.

3.2 Importance of Topography, River Network Structure, Geology, and Climate for Hydrologic Processes in Mountainous Terrains

In addition to the applied modeling work, we took the opportunity to address some fundamental theoretical questions. Topography, river network structure, geology, and climate control watershed response interactively in a hierarchical way (Jencso and McGlynn, 2011; Hale and McDonnell, 2016b). Our current results indicate that geological heterogeneity can enhance or diminish the effect of capturing topographic features on the simulated flow rate, mean age and solute concentration of baseflow. To further quantify the relationship between the hydrological response of mountainous watersheds and the landscape conditions including the structure of topography, topology and geometry of river network, geology, and climate, we create synthetic watersheds (Figures 3.8 and 3.9) with different river network structures and topographic characteristics. The channel network and topographic structure are characterized by Horton's stream number, stream length and drainage area ratio, as well as Tokunaga statistics (Figures 3.10 and 3.11). More metrics including the probability distribution function of slopes, lengths and areas of hillslopes of different orders, wavelength spectrum of topography (e.g. Perron et al., 2008), and the eigenvalue spectrum of the adjacency matrix of the network (e.g. Abed-Elmdoust et al., 2017), are being calculated to further quantify and distinguish different network and topography scenarios, and will be used in quantifying their effect on the simulated hydrological responses.

Some preliminary results are presented to show the surface and subsurface hydrological responses in synthetic watersheds with different channel networks and topographic structures (Figures 3.12, 3.13 and 3.14). Figure 3.12a shows that the channel network structure can have a significant influence on flood wave propagation in terms of the magnitude of the rising and recession limb, and time to peak of the hydrograph at

the outlet. Figure 3.12b shows the change of baseflow generated per unit stream area with stream order and the influence of channel network structure. Figures 3.13a and 3.14a show the baseflow recession processes in different synthetic watersheds, and Figures 3.13b and 3.14b show the change of recession rate with flow rate.

These results indicate that channel network and associated topographic structure can influence the simulated spatial and temporal distribution of baseflow generation, in addition to the commonly considered geological heterogeneity (Harman and Sivapalan, 2009). Baseflow recession analysis is fundamental to determine the constitutive storage-discharge relationship (e.g. Brutsaert and Nieber, 1977; Kirchner, 2009) and is critical to accurately estimate the recharge using parsimonious models (Ajami et al., 2011). Thus our results will be an important contribution to recharge estimation, especially for mountainous and data-sparse regions where landscape elevation data is far more easily accessed than geology data.
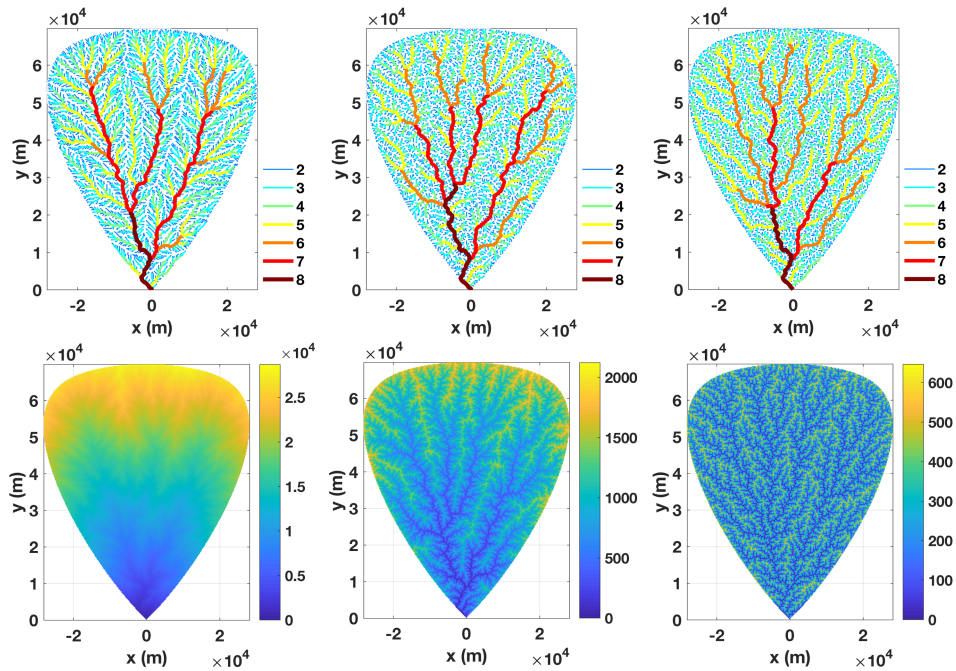
Figure 3.8: Synthetic river network with different structures (first row, $\alpha = -0.125, -0.5, -0.875$ from left to right) and associated topography (bottom row).
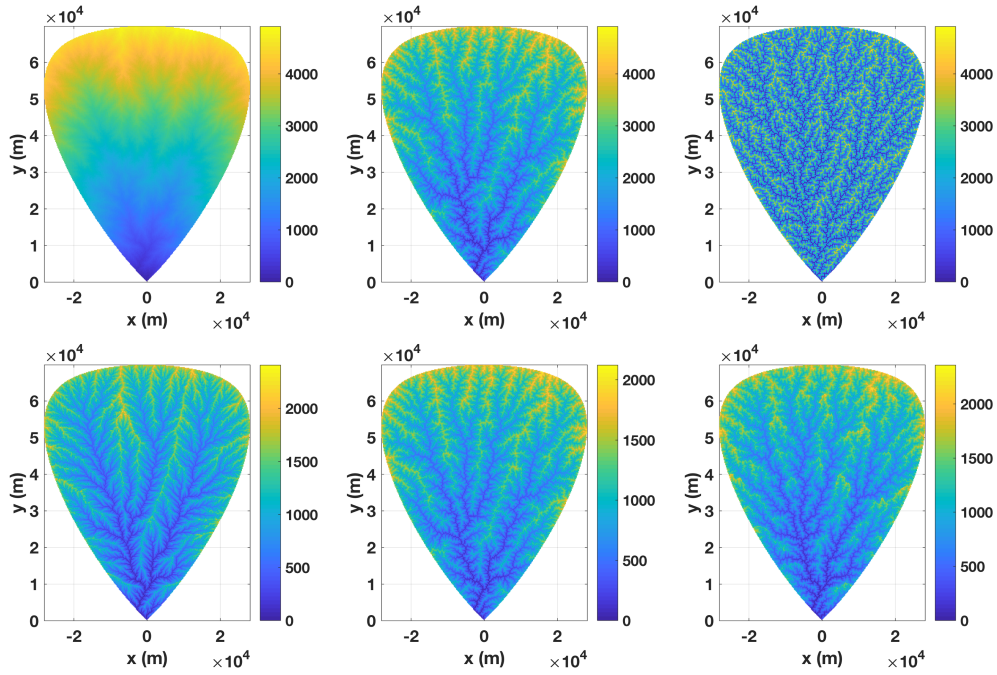
Figure 3.9: Linearly scaled (first row) and exponentially scaled (bottom row) OCN-DEM.
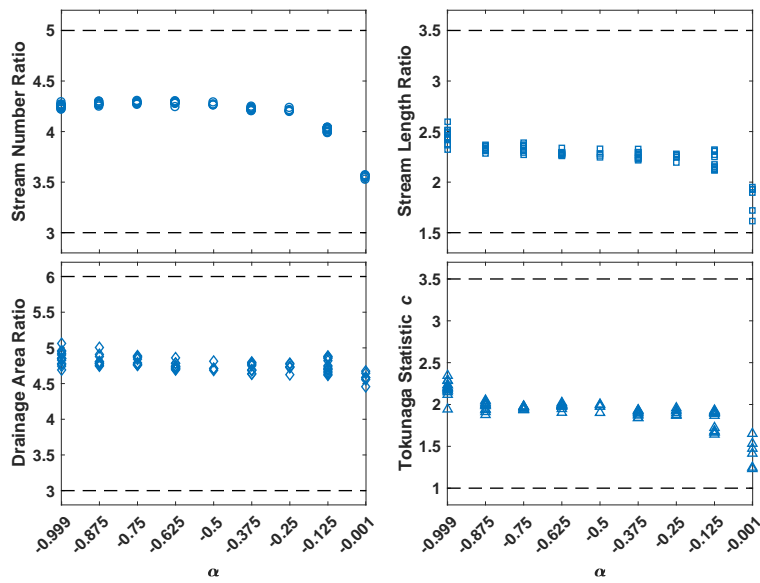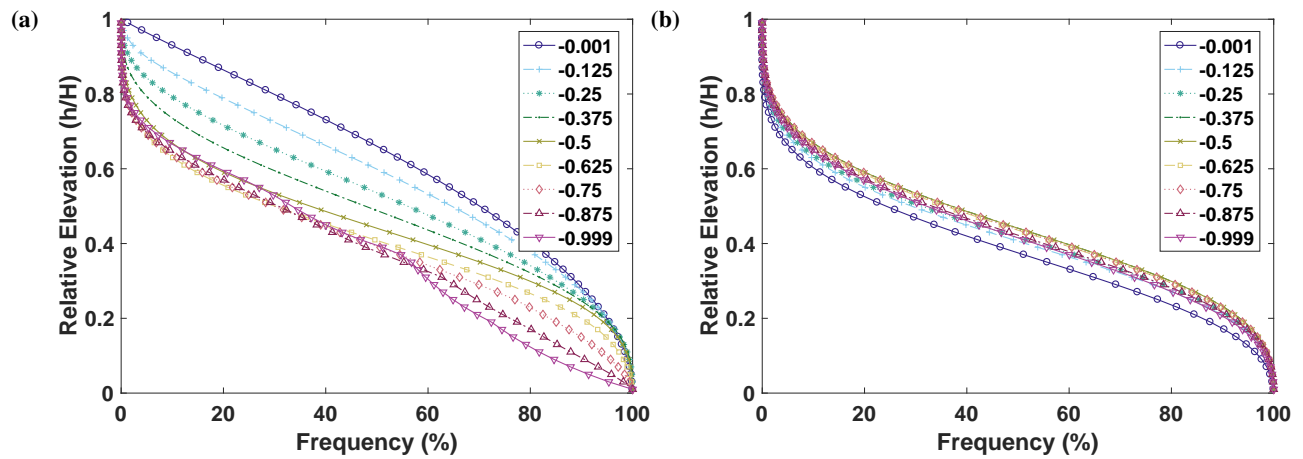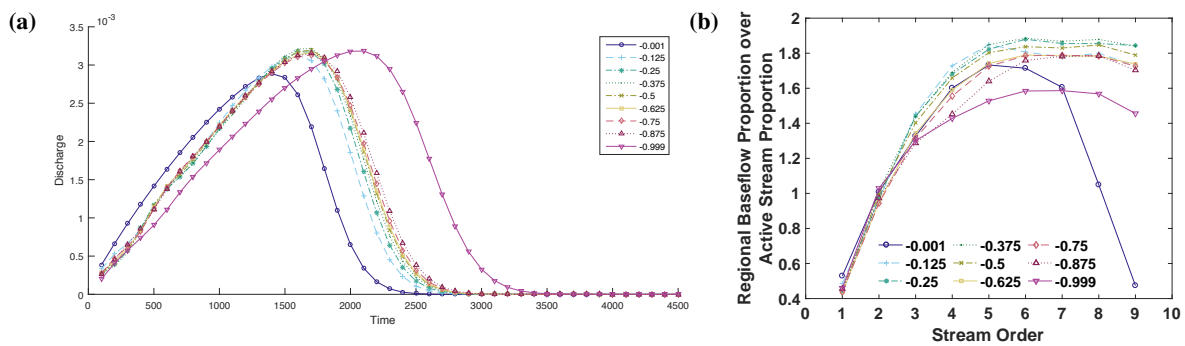

Figure 3.10: Statistics characterizing different channel network structures.

Figure 3.11: Hypsometric curve of OCN-DEM and linearly scaled OCN-DEM (a), and of exponentially scaled OCN-DEM (b) corresponding to OCN in Figure 3.8.

Figure 3.12: (a) Influence of river network structure on runoff routing through the river network. Different river network structures result in different unit hydrographs at the watershed outlet. (b) Spatial scaling of baseflow with drainage order and the influence of river network structure. Different river network structures correspond to different parameter values shown in the legend.
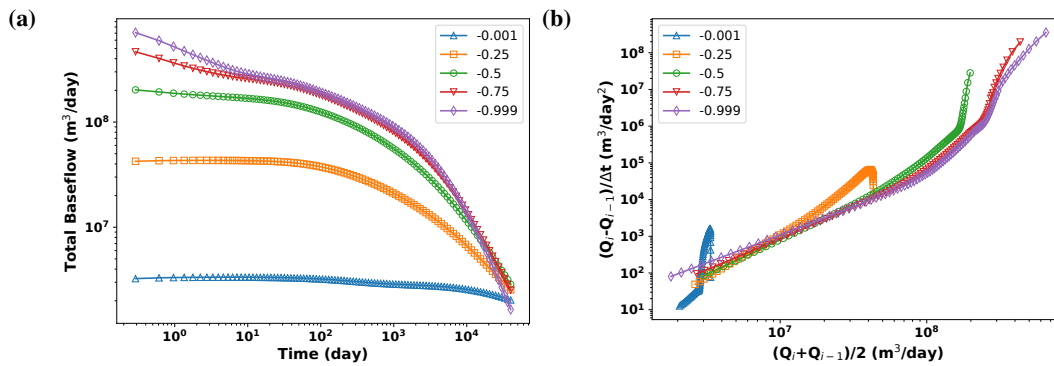
Figure 3.13: Control of channel network and topographic structure on baseflow recession. (a) Baseflow recession process starting from steady-state groundwater flow field using linearly scaled OCN-DEM. (b) Change of baseflow recession rate with flow rate.
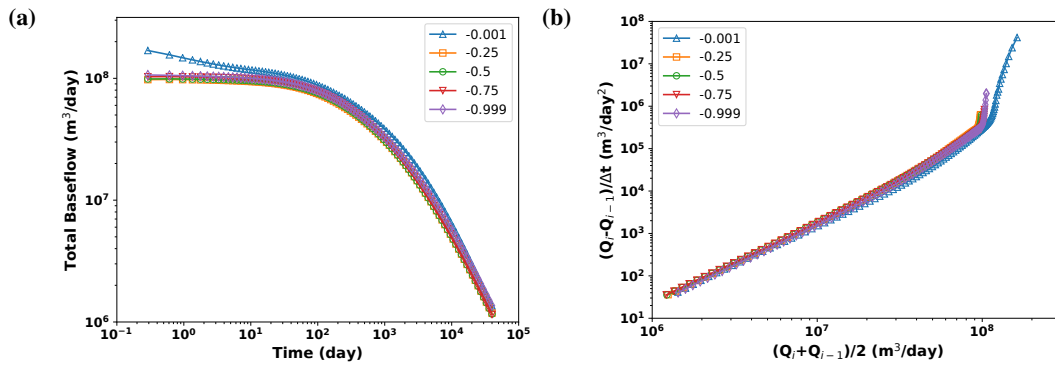
Figure 3.14: Control of channel network and topographic structure on baseflow recession. (a) Baseflow recession process starting from steady-state groundwater flow field using exponentially scaled OCN-DEM. (b) Change of baseflow recession rate with flow rate.

Chapter 4

SUMMARY AND CONCLUSIONS

Principal findings, conclusions, and recommendations with respect to water resources problems and recommendations for additional research or application

From the first part of the work, we find that even if the net response of the watershed is essentially the same, mesh characteristics, particularly the ability of the mesh to capture key topographic features such as streams and ridges, can significantly affect the spatial distribution of groundwater flow paths and the relative amount of baseflow generated at different scales. This, at the same time, strongly affects residence times and solute transport characteristics. Compared to the model with the highest TCL, which captures all the streams and ridges, low TCL models generally result in less flow through small scale local flow paths and more flow through large scale regional flow paths. This is reflected in lower baseflow into low-order streams and more baseflow into high-order streams. The spatial distribution of baseflow due to missing stream and ridge features can be up to 10% in low-order streams and 20% in high-order streams. This further has an effect of producing less young water into low-order streams and more old water into high-order streams, biasing the simulated age older for water into streams of all orders.

Our results indicate that representing streams and ridges in the numerical model is fundamental to reproducing accurately internal flow and transport characteristics within mountainous watersheds with complex topography. We are currently working on building a more realistic hydrogeologic conceptual model of the Rio Hondo watershed for further modeling. Based on the current results about the effect of complex topographic features, we will further investigate how the complex topography together with the fractured bedrock geology hierarchically control the hydrological processes within the mountain block and control the recharge from mountain block to mountain front aquifer.

The second part of the work focuses on building synthetic watersheds with different river network structure, topography, and geology to quantify the relationships between watershed structure and hydrological responses under different climate conditions. Our preliminary results show that the structure of the channel network and associated topography can significantly influence the simulated baseflow spatial distribution and baseflow recession. Baseflow recession analysis is critical to building a parsimonious model based on watershed storage-discharge relationships to estimate recharge. Thus our results will contribute to incorporating the topographic information into baseflow recession analysis and will improve the watershed storage-discharge relationship that is used in the parsimonious recharge estimation model.

Chapter 5

FUNDING PRODUCTS

5.1 Student and Post doc participation

- Chao Wang, PhD student in hydrology. Chao, the student funded under this grant, was awarded the Outstanding Teaching Award for the Dept. of Earth & Environmental Sciences in 2017. He also successfully passed his PhD Candidacy Exam.

- Manoj KC, Post doc in hydrology

5.2 Publication

Wang C., J. D. Gomez-Velez, and J. L. Wilson (2018), *The Importance of Capturing Topographic Features for Modeling Groundwater Flow and Transport in Mountainous Watersheds*, Water Resources Research 54(12): 10,313-10,338. This summarizes sections 3.1 and its associated methods.

5.3 Manuscripts

- Wang C., J. D. Gomez-Velez, and J. L. Wilson (2018), *The Importance of Topography, River Network Structure, Geology, and Climate for Hydrologic Processes in Mountainous Terrains*, In preparation for Geophysical Research Letters. This summarizes sections 3.2 and its associated methods.

- Gomez-Velez J.D. (2017), *Exploring the Dynamics of Hydrologic Response and Age Distributions*,

MS Thesis in Applied Mathematics, Mathematics Dept., New Mexico Tech. The mathematical theory for the parsimonious model described above was developed as part of this thesis.

5.4 Conference Presentations

Preliminary results of this research were presented at the following conferences:

- **Wang C.**, **J. D. Gomez-Velez**, and J. L. Wilson. The importance of capturing topographic features for modeling groundwater flow and transport in mountainous watersheds. 2017 AGU Annual Meeting, New Orleans, Louisiana. December 2017. Oral Presentation.

- **Gomez-Velez, J. D.**, J. W. Harvey, D. Scott, E. W. Boyer, and N. M. Schmadel, *Seasonal Dynamics of River Corridor Exchange Across the Continental United States*. Linking Dynamic Watershed Processes Across Spatial and Temporal Scales, 2017 AGU Annual Meeting, New Orleans, Louisiana. December 2017.

- **Gomez-Velez, J. D.** *The Earth's Arteries: Connectivity Along River Corridors*. Water Security and Sustainable Development Under Changing Environment, ESTDS2017, Nanjing, China. October, 2017.

- **Gomez-Velez, J. D.** *Leaky Pipes Everywhere! Understanding Connectivity Along River Corridors*. Dept. of Geosciences, University of Texas at El Paso, El Paso, Texas. October 2017.

- **Gomez-Velez, J. D.** *Leaky Pipes Everywhere! Understanding Connectivity Along River Corridors*. Plant & Environmental Sciences Department, New Mexico State University, Las Cruces, New Mexico. September 2017.

- **Gomez-Velez, J. D.** *Riverine Exchange Fluxes from Mountains to the Sea: Past, Present, and Future*. Sediments with Hydrodynamically Driven Flow, from Stream to Shelf. ASLO 2017 Aquatic Sciences Meeting, Honolulu, Hawaii. February 2017.

- **Gomez-Velez, J. D.**, J. W. Harvey, D. T. Scott, R. B. Alexander, and G. E. Schwarz. *Modeling hyporheic connectivity and water quality functions at the continental scale: implications for management*. Successes in integrating models and measurements into management for aquatic connectivity, 2017 AWRA Spring Specialty Conference. Connecting the Dots: The Emerging Science of Aquatic Systems Connectivity, Snowbird, Utah. April 2017.

- **Gomez-Velez, J. D.** *Conectividad en Corredores Fluviales: Pasado, Presente, y Futuro*. Dept. Environmental and Water Sciences, Sonora Institute of Technology, Ciudad Obregón, Mexico. March 2017.

- **Wang C.**, **J. D. Gomez-Velez**, and J. L. Wilson, *The Importance of Capturing Topographic Variability for Modeling Flow and Transport in Mountainous Terrains*, New Mexico Geological Society Annual Spring Meeting, Socorro, NM, 2016.

- **Gomez-Velez, J. D.** *From bedforms to basins: Upscaling hyporheic exchange to understand connectivity in large river networks*. Biological Systems Engineering Department, Virginia Tech, Blacksburg, Virginia. October 2015.

5.5 Proposals

Preliminary results of this research led to the following proposals:

- NSF-Division of Earth Sciences: *Using Magnetotellurics to Understand Deep Circulation in Regional Flow Systems*. 2018-2021. US$ 500,000 (PI). Under Review.

- USGS: *An Operational Framework to Estimate High-resolution Water Fluxes: Combining Physics-Based Models, Geophysical Observations, and Satellite Imagery*. 2017-2020. US$ 250,000 (co-PI). Not Funded.

  NASA: *An Operational Framework to Estimate High-resolution Water Fluxes in the Semiarid Southwest: Combining Physics-Based Models, Satellite Imagery, and Geophysical Observations*. US$ 1,000,000 (PI). Not Funded and resubmission in progress.

- EPSCoR Innovative Working Group: *Optimizing the Use of New Mexico's Renewable Energy and Water Resources*. 2016. US$ 7,500 (Co-PI)

5.6 New Courses

I designed the course **HYD 520/GEOP 520/MATH 583 Data-driven Modeling in Science and Engineering**. This course introduces students to statistical learning techniques and data assimilation for science and engineering applications. Given the wide variety of topics, the course focuses on practical applications and

emphasizes the understanding of the assumptions underlying different techniques. This approach allows students to learn the basics of useful tools for data-driven modeling and revisit their theoretical and practical underpinnings as needed. Topics may include supervised and unsupervised learning, regression, classification, importance sampling, ensemble forecasting, and Kalman Filtering. The codes R or Python will be used for the class.

Bibliography

Abed-Elmdoust, A., M.-A. Miri, and A. Singh (2016, November). Reorganization of river networks under changing spatiotemporal precipitation patterns: An optimal channel network approach. *Water Resour. Res. 52*(11), 8845–8860.

Abed-Elmdoust, A., A. Singh, and Z.-L. Yang (2017, September). Emergent spectral properties of river network topology: an optimal channel network approach. *Scientific Reports 7*(1), 11486.

Ajami, H., P. A. Troch, T. Maddock, T. Meixner, and C. Eastoe (2011, April). Quantifying mountain block recharge by means of catchment-scale storage-discharge relationships. *Water Resour. Res. 47*(4), W04504.

Aquanty (2016). HydroGeoSphere Manual.

Beven, K. and P. Germann (1982, October). Macropores and water flow in soils. *Water Resour. Res. 18*(5), 1311–1325.

Beven, K. and P. Germann (2013, June). Macropores and water flow in soils revisited. *Water Resour. Res. 49*(6), 3071–3092.

Brunner, P. and C. T. Simmons (2012, March). HydroGeoSphere: A Fully Integrated, Physically Based Hydrological Model. *Ground Water 50*(2), 170–176.

Brutsaert, W. and J. L. Nieber (1977, June). Regionalized drought flow hydrographs from a mature glaciated plateau. *Water Resour. Res. 13*(3), 637–643.

Cardenas, M. B. and X.-W. Jiang (2010, November). Groundwater flow, transport, and residence times through topography-driven basins with exponentially decreasing permeability and porosity. *Water Resour. Res. 46*(11), W11538.

Dingman, S. L. (2015). *Physical Hydrology* (3rd ed.). Waveland Press.

Freeze, R. A. and P. A. Witherspoon (1967, June). Theoretical analysis of regional groundwater flow: 2. Effect of water-table configuration and subsurface permeability variation. *Water Resour. Res. 3*(2), 623–634.

Frisbee, M. D., F. M. Phillips, A. R. Campbell, F. Liu, and S. A. Sanchez (2011, June). Streamflow generation in a large, alpine watershed in the southern Rocky Mountains of Colorado: Is streamflow generation simply the aggregation of hillslope runoff responses? *Water Resour. Res. 47*(6), W06512.

Frisbee, M. D., D. G. Tolley, and J. L. Wilson (2017, April). Field estimates of groundwater circulation depths in two mountainous watersheds in the western U.S. and the effect of deep circulation on solute concentrations in streamflow. *Water Resour. Res. 53*(4), 2693–2715.

Ginn, T. R. (1999, May). On the distribution of multicomponent mixtures over generalized exposure time in subsurface flow and reactive transport: Foundations, and formulations for groundwater age, chemical heterogeneity, and biodegradation. *Water Resources Research 35*(5), 1395–1407.

Gleeson, T. and A. H. Manning (2008, October). Regional groundwater flow in mountainous terrain: Three-dimensional simulations of topographic and hydrogeologic controls. *Water Resour. Res. 44*(10), W10403.

Gomez, J. D. and J. L. Wilson (2013, March). Age distributions and dynamically changing hydrologic systems: Exploring topography-driven flow. *Water Resour. Res. 49*(3), 1503–1522.

Gomez-Velez, J. D., S. Krause, and J. L. Wilson (2014, June). Effect of low-permeability layers on spatial patterns of hyporheic exchange and groundwater upwelling. *Water Resour. Res. 50*(6), 5196–5215.

Goode, D. (1996). Direct simulation of groundwater age. *Water Resour. Res. 32*(2), 289–296.

Haitjema, H. M. and S. Mitchell-Bruker (2005, November). Are Water Tables a Subdued Replica of the Topography? *Ground Water 43*(6), 781–786.

Hale, V. C. and J. J. McDonnell (2016a, February). Effect of bedrock permeability on stream base flow mean transit time scaling relations: 1. A multiscale catchment intercomparison. *Water Resour. Res. 52*(2), 1358–1374.

Hale, V. C. and J. J. McDonnell (2016b, February). Effect of bedrock permeability on stream base flow mean transit time scaling relations: 1. A multiscale catchment intercomparison. *Water Resour. Res. 52*(2), 1358–1374.

Harbaugh, A. W. (2005). MODFLOW-2005, the U.S. Geological Survey modular ground-water model – the Ground-Water Flow Process. Technical Report U.S. Geological Survey Techniques and Methods 6-A16.

Harman, C. and M. Sivapalan (2009, January). Effects of hydraulic conductivity variability on hillslope-scale shallow subsurface flow response and storage-discharge relations. *Water Resour. Res. 45*(1), W01421.

Hooshyar, M., A. Singh, and D. Wang (2017, May). Hydrologic controls on junction angle of river networks. *Water Resources Research 53*(5), 4073–4083.

Horton, R. E. (1932, June). Drainage-basin characteristics. *Eos Trans. AGU 13*(1), 350–361.

Ingebritsen, S. E. and C. E. Manning (1999, December). Geological implications of a permeability-depth curve for the continental crust. *Geology 27*(12), 1107–1110.

Jencso, K. G. and B. L. McGlynn (2011, November). Hierarchical controls on runoff generation: Topographically driven hydrologic connectivity, geology, and vegetation. *Water Resour. Res. 47*(11), W11527.

Kirchner, J. W. (2009, February). Catchments as simple dynamical systems: Catchment characterization, rainfall-runoff modeling, and doing hydrology backward. *Water Resour. Res. 45*(2), W02429.

Liu, J., X. Chen, H. Lin, H. Liu, and H. Song (2013, November). A simple geomorphic-based analytical model for predicting the spatial distribution of soil thickness in headwater hillslopes and catchments. *Water Resour. Res. 49*(11), 7733–7746.

Louis, C. (1972). Rock Hydraulics. In *Rock Mechanics*, International Centre for Mechanical Sciences, pp. 299–387. Springer, Vienna. DOI: 10.1007/978-3-7091-4109-0_16.

Maher, K. (2011, December). The role of fluid residence time and topographic scales in determining chemical fluxes from landscapes. *Earth and Planetary Science Letters 312*(1–2), 48–58.

Maher, K. and C. P. Chamberlain (2014, March). Hydrologic Regulation of Chemical Weathering and the Geologic Carbon Cycle. *Science 343*(6178), 1502–1504.

McGuire, K. J., C. E. Torgersen, G. E. Likens, D. C. Buso, W. H. Lowe, and S. W. Bailey (2014, May). Network analysis reveals multiscale controls on streamwater chemistry. *PNAS 111*(19), 7030–7035.

Peckham, S. (2015). Longitudinal Elevation Profiles of Rivers: Curve Fitting with Functions Predicted by Theory. In *Geomorphometry for Geosciences*, pp. 137 – 140. Poznań, Poland: Bogucki Wydawnictwo Naukowe, Adam Mickiewicz University in Poznań - Institute of Geoecology and Geoinformation.

Perron, J. T., J. W. Kirchner, and W. E. Dietrich (2008, December). Spectral signatures of characteristic spatial scales and nonfractal structure in landscapes. *Journal of Geophysical Research: Earth Surface 113*(F4), F04003.

Perron, J. T., P. W. Richardson, K. L. Ferrier, and M. Lapôtre (2012, December). The root of branching river networks. *Nature 492*(7427), 100–103.

Rigon, R., M. Bancheri, G. Formetta, and A. de Lavenne (2016, January). The geomorphological unit hydrograph from a historical-critical perspective. *Earth Surf. Process. Landforms 41*(1), 27–37.

Rinaldo, A., A. Marani, and R. Rigon (1991, April). Geomorphological dispersion. *Water Resour. Res. 27*(4), 513–525.

Rinaldo, A., R. Rigon, J. R. Banavar, A. Maritan, and I. Rodriguez-Iturbe (2014, February). Evolution and selection of river networks: Statics, dynamics, and complexity. *PNAS 111*(7), 2417–2424.

Rodríguez-Iturbe, I. and A. Rinaldo (1997). *Fractal River Basins: Chance and Self-Organization*. Cambridge University Press.

Saar, M. O. and M. Manga (2004, April). Depth dependence of permeability in the Oregon Cascades inferred from hydrogeologic, thermal, seismic, and magmatic modeling constraints. *J. Geophys. Res. 109*(B4), B04204.

Sun, T., P. Meakin, and T. Jøssang (1994, September). The topography of optimal drainage basins. *Water Resour. Res. 30*(9), 2599–2610.

Tarboton, D. G., R. L. Bras, and I. Rodriguez-Iturbe (1989, September). Scaling and elevation in river networks. *Water Resour. Res. 25*(9), 2037–2051.

Tarboton, D. G., R. L. Bras, and I. Rodriguez-Iturbe (1991, January). On the extraction of channel networks from digital elevation data. *Hydrological Processes 5*(1), 81–100.

Therrien, R., R. McLaren, E. Sudicky, and S. Panday (2010). Hydrogeosphere: a three-dimensional numerical model describing fully-integrated subsurface and surface flow and solute transport. *Groundwater Simulations Group, University of Waterloo, Waterloo, ON*.

Tolley, D. G. (2014, May). *High-Elevation Mountain Streamflow Generation: The Role of Deep Groundwater in the Rio Hondo Watershed, Northern New Mexico*. MS Thesis, New Mexico Institute of Mining and Technology, Socorro, New Mexico, USA.

Tolley, D. G., M. D. Frisbee, and A. R. Campbell (2015). Determining the importance of seasonality on groundwater recharge and streamflow in the Sangre de Cristo Mountains using stable isotopes. In *Geology of the Las Vegas Region*, Volume Guidebook, 66th Field Conference, pp. 303–312. New Mexico Geological Society.

Tóth, J. (1963, August). A theoretical analysis of groundwater flow in small drainage basins. *J. Geophys. Res. 68*(16), 4795–4812.

Tóth, J. (2009). *Gravitational systems of groundwater flow: Theory, Evaluation, Utilization*. Cambridge University Press.

Tromp-van Meerveld, H. J. and J. J. McDonnell (2006, February). Threshold relations in subsurface stormflow: 2. The fill and spill hypothesis. *Water Resour. Res. 42*(2), W02411.

Varni, M. and J. Carrera (1998). Simulation of groundwater age distributions. *Water Resour. Res. 34*(12), 3271–3281.

Zlotnik, V. A., M. B. Cardenas, and D. Toundykov (2011, July). Effects of Multiscale Anisotropy on Basin and Hyporheic Groundwater Flow. *Ground Water 49*(4), 576–583.